

AD-A047 303

RAYTHEON CO PORTSMOUTH R I SUBMARINE SIGNAL DIV
PARAMETRIC SONAR STUDY NEAR-FIELD INVESTIGATION, (U)
JUL 77 J C LOCKWOOD

F/G 17/1

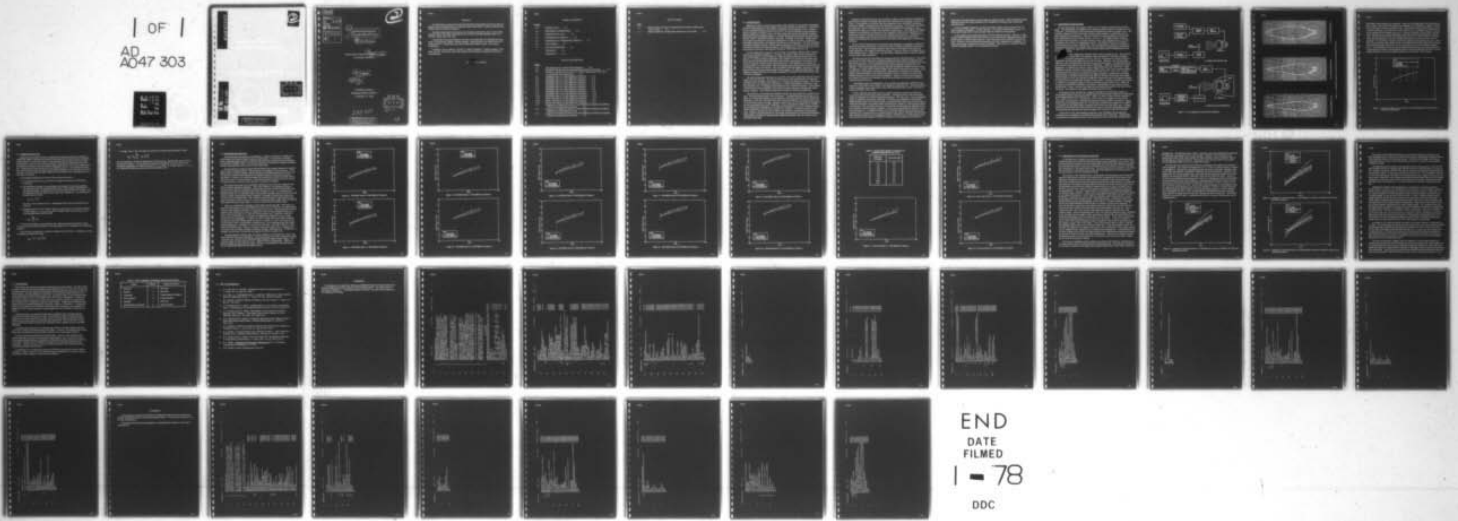
UNCLASSIFIED

R1706

N00024-76-C-6051

NL

| OF |
AD
A047 303



END
DATE
FILMED
1 - 78
DDC

AD A 0 47303

②
B.S.

AD No. _____
DDC FILE COPY

DDC
RECEIVED
DEC 6 1977
RESERVED
D

DISTRIBUTION STATEMENT A

Approved for public release;
Distribution Unlimited

14 R1786

2

ACCESSION for	
NTIS	White Section <input checked="" type="checkbox"/>
DDC	Buf Section <input type="checkbox"/>
UNANNOUNCED <input type="checkbox"/>	
JUSTIFICATION	
Per file on file	
BY	
DISTRIBUTION/AVAILABILITY CODES	
Dist.	AVAIL. and/or SPECIAL
A	

6
PARAMETRIC SONAR STUDY
NEAR-FIELD INVESTIGATION

10
Dr. James C./Lockwood

15
Prepared under Contract No. ~~N00024-76-C-6051~~
for NAVSEA Code 06H1-1

11
29 July 1977

12
49p.

RAYTHEON COMPANY
SUBMARINE SIGNAL DIVISION
Portsmouth, RI 02871

DDC
RECEIVED
DEC 6 1977
4 D

298 125

DISTRIBUTION STATEMENT A
Approved for public release;
Distribution Unlimited

1B

PREFACE

The opportunity to perform this Nearfield Parametric Sonar Study was made possible by adding a series of measurements to a Special Purpose Sonar (SPS) Transducer Measurement Program that was already in progress.

Nearfield measurements were made at the Transducer Evaluation Center, Naval Ocean Systems Center, San Diego, California and at the Naval Underwater Systems Center Test Facility, Seneca Lake, New York.

I am grateful to the help extended to me both in collecting data and critiquing this report by Dr. George Walsh, Messrs. William Backman, James Bartram, and Dennis McCrady of Raytheon; and Dr. Mark Moffet of the Naval Underwater Systems Center, New London, Connecticut.

In addition I wish to thank Mr. Herbert C. Single of Raytheon, Program Manager of this study, and Mr. John Neely, Code 06H1 NAVSEA, who authorized and funded the work that was performed.

Dr.  C. Lockwood

TABLE OF CONTENTS

Section

1.0	INTRODUCTION . . . 1-1
2.0	EXPERIMENT DESCRIPTIONS . . . 2-1
3.0	CORRECTION OF DATA . . . 3-1
4.0	EXPERIMENTAL RESULTS . . . 4-1
5.0	COMPARISON OF THEORETICAL RESULTS . . . 5-1
6.0	CONCLUSIONS . . . 6-1
7.0	LIST OF REFERENCES . . . 7-1
	APPENDIX A . . . A 1
	APPENDIX B . . . B 1

LIST OF ILLUSTRATIONS

Figure

2-1	Test Configuration Functional Block Diagrams . . . 2-2
2-2	TRANSDEC Beampatterns Demonstrating Intermodulation Distortion . . . 2-3
2-3	Secondary Frequency Source Level at 1.5 kHz as Measured for Four Drive Levels (Seneca Lake Experiment) . . . 2-4
4-1	TRANSDEC Data at 1.0 kHz Difference Frequency . . . 4-2
4-2	TRANSDEC Data at 1.5 kHz Difference Frequency . . . 4-2
4-3	TRANSDEC Data at 2.0 kHz Difference Frequency . . . 4-3
4-4	TRANSDEC Data at 2.5 kHz Difference Frequency . . . 4-3
4-5	TRANSDEC Data at 3.0 kHz Difference Frequency . . . 4-4
4-6	TRANSDEC Data at 4.0 kHz Difference Frequency . . . 4-4
4-7	TRANSDEC Data at 6.0 kHz Difference Frequency . . . 4-5
4-8	TRANSDEC Data at 8.0 kHz Difference Frequency . . . 4-5
4-9	TRANSDEC Data at 10.0 kHz Difference Frequency . . . 4-6
4-10	TRANSDEC Data at 12.0 kHz Difference Frequency . . . 4-6
4-11	Seneca Lake Data at 1.5 kHz Difference Frequency . . . 4-7
4-12	Seneca Lake Data at 2.5 kHz Difference Frequency . . . 4-8
4-13	Seneca Lake Data at 3.0 kHz Difference Frequency . . . 4-8
5-1	Comparison of Theoretical Data for 1.5 kHz Difference Frequency (Conditions of Seneca Lake Experiment Assumed) . . . 5-2
5-2	Comparison of Theoretical Data for 3.0 kHz Difference Frequency (Conditions of Seneca Lake Experiment Assumed) . . . 5-3
5-3	Comparison of Theoretical Data for 10.0 kHz Difference Frequency (Conditions of Seneca Lake Experiment Assumed) . . . 5-3

LIST OF TABLES

Table

4-1	Measured Data Increases to Compensate for Assumed Constant Mean Source Level . . . 4-7
6-1	Degree of Difficulty and Equipment Required for Each Model . . . 6-2

1.0 INTRODUCTION

Difference frequency sound pressure levels in the nearfield of a parametric transmitting array have been measured in two separate experiments with the same projector. The projector has a nearfield distance at the primary frequencies of approximately 6.0 m. Measurements were made at ranges of from 3.0 to 24.0 m, in order to show the nearfield buildup of apparent difference frequency source level from within the projector's nearfield to approximately four times its nearfield distance. The first experiment took place at the Naval Ocean Systems Center's TRANSDEC facility in San Diego, California in July 1976. Measurements were made at ten difference frequencies ranging from 1.0 kHz to 12.0 kHz. In these and succeeding measurements, the projector was driven at two frequencies. The lower frequency remained a constant 42.58 kHz, and the higher frequency was varied from 43.58 to 54.58 kHz to produce the desired difference frequency. The downshift ratio, defined as the ratio of the mean primary frequency to the difference frequency, varied from 43.08 to 4.05.

The data obtained at a range of 24.0 m and some of the higher-frequency data at shorter ranges were considered satisfactory. However, the shorter-range, lower-frequency data were contaminated by receiver distortion, which was apparent from the shape of the beam-patterns. It is believed that the hydrophone used, because it is of the electrostrictive type, has an inherent intermodulation distortion response that is proportional to the square of the primary frequency pressure at the measurement point. If the dependence on primary frequency pressure is in fact quadratic, then the distortion level must increase at a rate of 40.0 dB per decade as range is decreased. Thus a hydrophone showing negligible distortion at ranges greater than 24.0 m may be totally unusable at short ranges or at large downshift ratios. This suggests a fundamental limit to the useful combination of downshift ratios and nearfield range for a given hydrophone.

The second experiment took place in April 1977 at the Naval Underwater Systems Center's Seneca Lake Test Facility. The objective of the Seneca Lake experiment was to repeat the conditions of the TRANSDEC experiment and to overcome the distortion problem. The distortion was hoped to be eliminated by substitution of a different hydrophone, preferably, a non-electrostrictive one. If changing the hydrophone failed to resolve the problem, it was planned to cover the face of the hydrophone with a sound absorbing material to attenuate the intense primary radiation. The distortion would then be expected to diminish quadratically.

The objective of overcoming the distortion problem was not realized for a number of reasons. The major obstacle was a lack of test time. The nearfield measurements were to be taken as a low-priority addition to a test program in which the emphasis was on farfield measurements. In the end, only about three hours became available for nearfield measurements out of over three weeks of testing. Because of lack of time, it was not possible to attempt the use of a sound absorber to cut the distortion. It was not possible to obtain use of a suitable non-electrostrictive hydrophone, so the best that could be done was to use a different electrostrictive hydrophone and hope that it would be less nonlinear. Such did not prove to be the case. However, because time was so short it was decided to concentrate on taking axial levels and not to take beam patterns for all ranges and frequencies as was done at TRANSDEC. Consequently, the degree to which distortion affected the Seneca Lake test results was not determined until later.

Because no distortion-free data set was obtained, efforts were directed at evaluating the data that were obtained to establish which data were reliable and see if the data could be corrected. It was apparent for example, that the beampatterns from TRANSDEC revealed by their shape whether a substantial amount of distortion was present. It was further noted that the signal level could be estimated from the distorted beampatterns by fairing in a more characteristic shape in the vicinity of the maximum response axis. The method of identifying distortion and estimating corrections from the beampattern shape was not regarded as very satisfactory because it relied too heavily on the judgment of the observer. Furthermore, it could not be applied to the data taken at Seneca Lake because patterns were not made. Methods of estimating the distortion level and correcting the data analytically were therefore examined.

By use of the assumptions that the distortion level dependence is quadratic, and that the distortion and signal add in phase, it has been possible to deduce the distortion levels and to correct the data. The corrections depend to some extent on assumptions made about the range dependence of the signal as predicted by theory. However, there is no reliance on predicted absolute levels. Furthermore, only the shortest range data point is seriously affected by the assumed range dependence.

The data from the two experiments are compared with two nearfield theories. Then these two and several other theories are compared among themselves and their similarities and differences are noted. The first published theoretical treatment of the parametric array nearfield was included in the more general numerical volume integration model of Muir and Willette¹. The volume integration program originally developed by Willette has been revised by Lockwood to include finite-amplitude effects and to improve numerical convergence. In its modified form, the program was used by Muir, Mellenbruch and Lockwood² to model the unusual nearfield geometry of the reflected parametric array. Lockwood's version of the Willette program is used in the present investigation. However, for the cases considered, the results are believed to be identical to those that would have been obtained had Willette's original program been used.

An analytical model of the parametric array nearfield was published by Berkday³ in the same year (1972) that the Muir-Willette work appeared in published form. Because Berkday's model is applicable only to parametric arrays with collimated primary waves, it will not be considered further in this work.

In 1974, Bartram and Fugitt⁴ reported a simple closed-form model for a parametric array with conical piston beam primary radiations. Assumptions used in that work include neglect of absorption and of finite-amplitude attenuation. The same year, a more complicated analytical model was reported by Lockwood⁵. Presented as an adaptation of the (farfield) Mellen-Moffett⁶ model, the Lockwood model uses geometrically derived correction factors to modify the amplitudes of secondary signals emanating from ranges for which nearfield effects are important. The correction factors are derived under the assumption of negligible losses in the interval to which the factor is applied. Losses occurring outside that interval are properly accounted for. A significant feature of the Lockwood model is that it accounts for the transition from a conical beam to a cylindrical beam at the primary frequency nearfield limit. Other models are based on the assumption of either a cylindrical or a conical primary beam. (The Bartram⁴ model contains a cylindrical nearfield in its formulation, but its effect is

suppressed in an approximation used to obtain the reported result.) Both the Bartram and the Lockwood models have been evaluated for the conditions of the Seneca Lake experiments reported herein.

In 1975, Rolleigh⁷ published a nearfield model that includes explicit account of the primary frequency beampattern. In other respects, it is similar to the Bartram⁴ model. Its major shortcoming is that it does not apply within the nearfield of the projector.

In two recent works, nearfield absorption has been taken into account. The first, a 1975 work of Mellen⁸ actually contains two models, one for cylindrically collimated primary waves and the other for conical beam primaries. Both models have been evaluated in the present work. However, for the parameters considered, the effect of attenuation is negligible. The most recent model reported is by Mellen and Moffett⁹. This model is, in concept, closely related to Rolleigh's model⁷, but is evaluated numerically.

2.0 EXPERIMENT DESCRIPTIONS

The two experiments, the results of which are to be reported, both took place in fresh water. The experiments at TRANSDEC were conducted with the projector at a depth of 5.44 m in the tank. A block diagram of the experimental arrangement is shown in Figure 2-1(a). The projector, effectively a 20-inch diameter circular piston transducer, radiated the two primary frequencies simultaneously. The lower frequency was held constant at 42.50 kHz and had a measured source level of 226.2 dB re 1 μ Pa at 1 m. The higher primary frequency was varied from 43.58 kHz to 54.58 kHz and had a source level varying from 221.3 to 227.8 depending on the projector's transmitting response. The signals from the two oscillators were summed prior to power amplification. The receiving system consisted of an NUSC XU-1313 hydrophone followed by a lowpass filter and preamplifier and the standard TRANSDEC electronics. Output was channelled to a polar plotter, which produced beampatterns for all of the measurements.

The experimental configuration at Seneca Lake is shown in Figure 2-1(b). The projector, the projector behind a sonar dome, was suspended from the Transducer Calibration Platform (TCP) barge at a depth of approximately 76.0 m. The TCP electronics are similar to those at TRANSDEC and the preamp/filter box used was the same. Therefore, the only important difference in the receiving system was the use of an F-50 hydrophone. The signal generation used at Seneca Lake differed from that used at TRANSDEC. Rather than adding two primary frequencies, a modulator was used to produce single sideband (f_2) plus carrier (f_1). Other differences were the operation of the projector behind a dome, and a more powerful amplifier producing a primary source level outside the dome of 233.8 dB re 1 μ Pa at 1 m. For the measurements, the dome was positioned at the angle resulting in minimum beam distortion. Measurements at TRANSDEC indicated that the effect of the dome at this angle was to attenuate the primary source level and that the difference frequency source level seemed to behave as it should for the corresponding reduction in drive power. Therefore, the effect of the dome is believed to be negligible except to reduce the effective primary source level. Unlike the procedure followed in the TRANSDEC experiments, beampatterns were not drawn for each measurement. Rather, the beam was peaked up on the hydrophone and the axial source level was noted. The reason for this change of procedure was lack of time.

As mentioned in the introduction, during the TRANSDEC experiment the presence of intermodulation distortion in the receiving hydrophone was noted at short ranges and low frequencies by examining the shapes of the beampatterns. Figure 2-2 shows a rather extreme example of this. Figure 2-2(c) is the 1.5 kHz pattern at 24.0 m and is representative of the normal appearance of the parametric nearfield beampatterns showing no effect of distortion. Figure 2-2(b) is the corresponding pattern at 6.0 m and shows considerable elongation at the pattern tip caused by the very high primary frequency levels in the area of the major lobe. In figure 2-2(a), the 3.0 m pattern, the primary levels have become so high that intermodulation distortion dominates the parametrically generated signal even in the area of the first sidelobes.

The presence of the intermodulation distortion in the TRANSDEC data provided the motivation for the acquisition of nearfield data during the Seneca Lake tests. Unfortunately, very little was accomplished at Seneca Lake because there was so little time available after

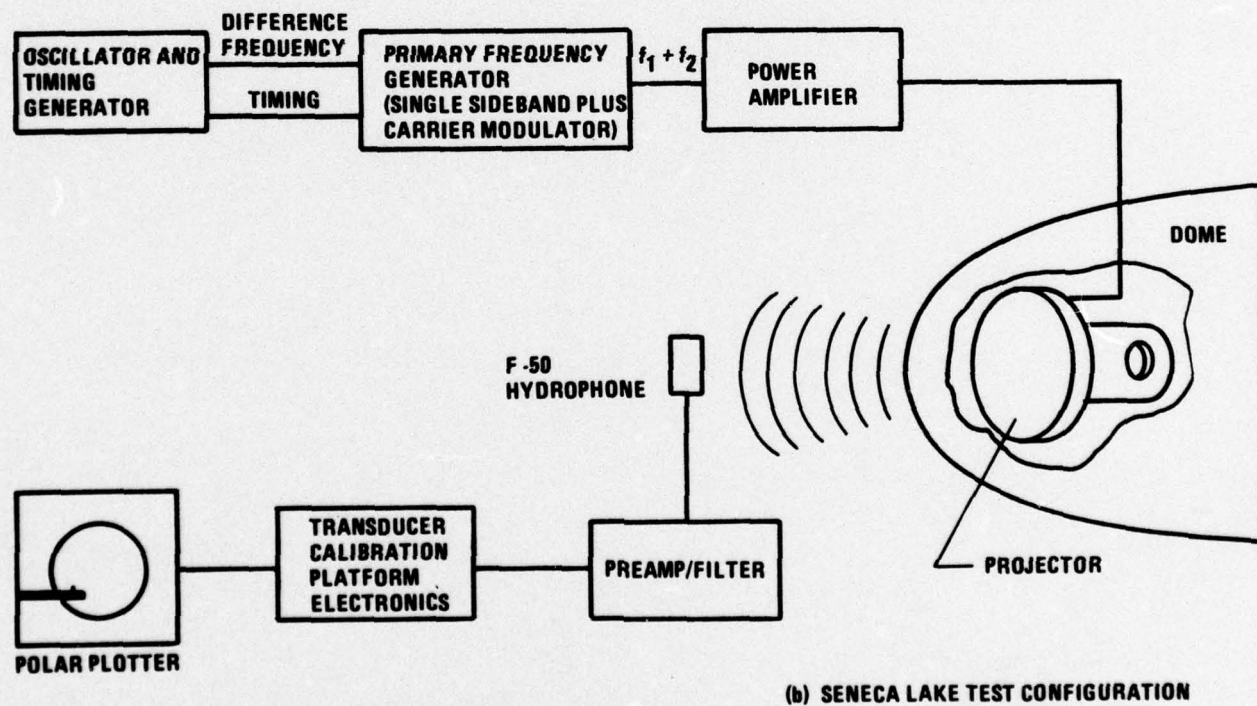
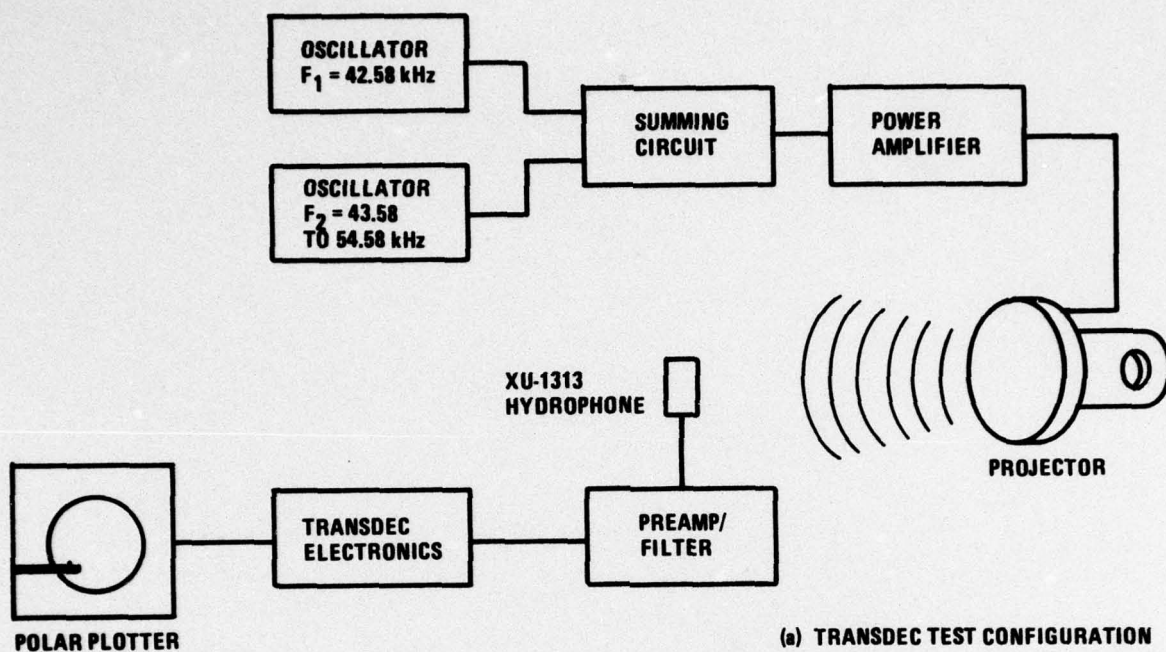
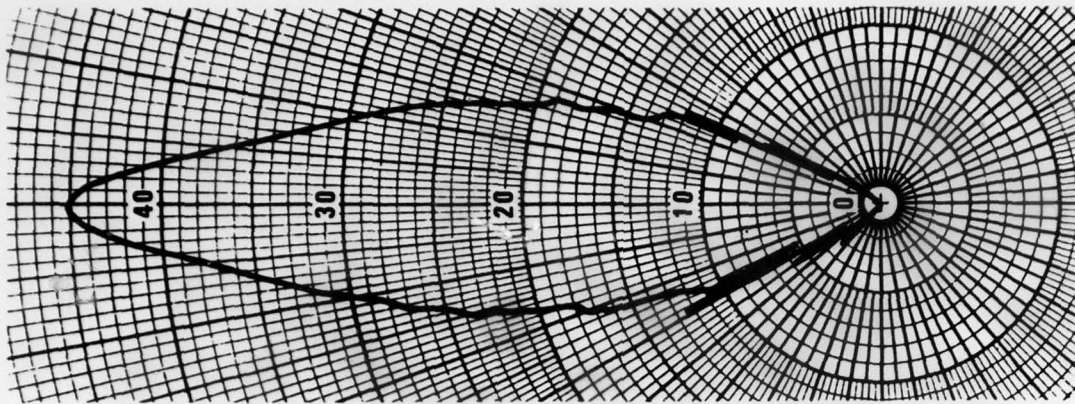
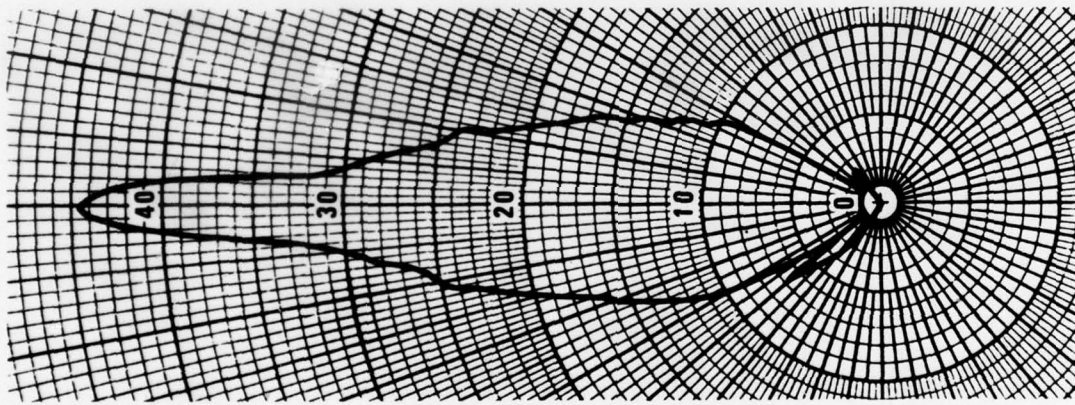


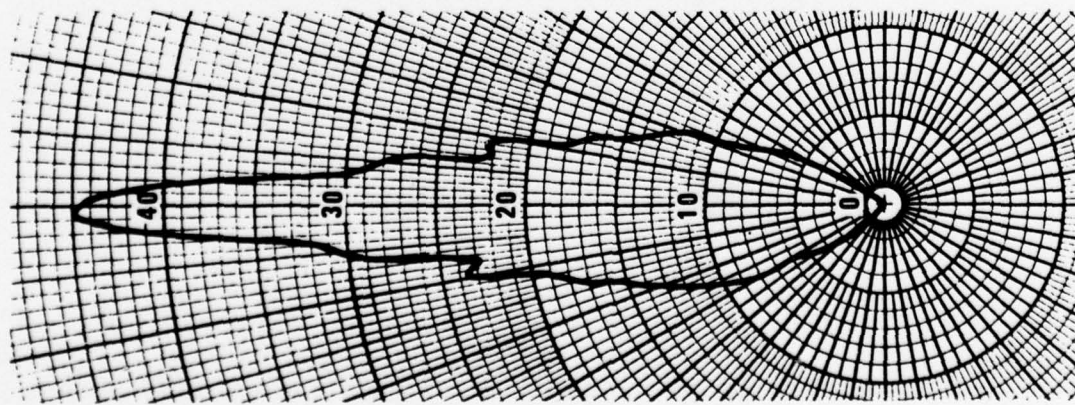
Figure 2-1. Test Configuration Functional Block Diagrams



(a) 1.5 kHz PATTERN AT 3.0 m



(b) 1.5 kHz PATTERN AT 6.0 m



(c) 1.5 kHz PATTERN AT 24.0 m

Figure 2-2. TRANSDEC Beampatterns Demonstrating Intermodulation Distortion

the farfield measurements were completed. There was one significant point demonstrated at Seneca Lake. That point was the power law dependence of the distortion. Figure 2-3 shows the 1.5 kHz data as measured at Seneca Lake. The data were taken at four primary source levels in 3.0 dB steps. The solid line is the theoretical curve according to the Muir-Willette¹ model evaluated for the highest source level. The great disparity between theory and experiment, particularly in the range dependence of the data, indicates that distortion is significant. The fact that the data for succeeding primary levels are almost exactly 6.0 dB apart shows that the dependence of the sum of signal and distortion on primary source level is quadratic. The parametric signal is known to be a quadratic function of primary level. Therefore, the fact that the range dependence does not change with primary source level indicates that the intermodulation distortion, is also a quadratic function of the primary frequency level. This demonstration that the intermodulation distortion goes as the square of the primary frequency pressure at the hydrophone makes it possible to attribute a 40.0 dB per decade range dependence to the intermodulation distortion in the farfield of the projector.

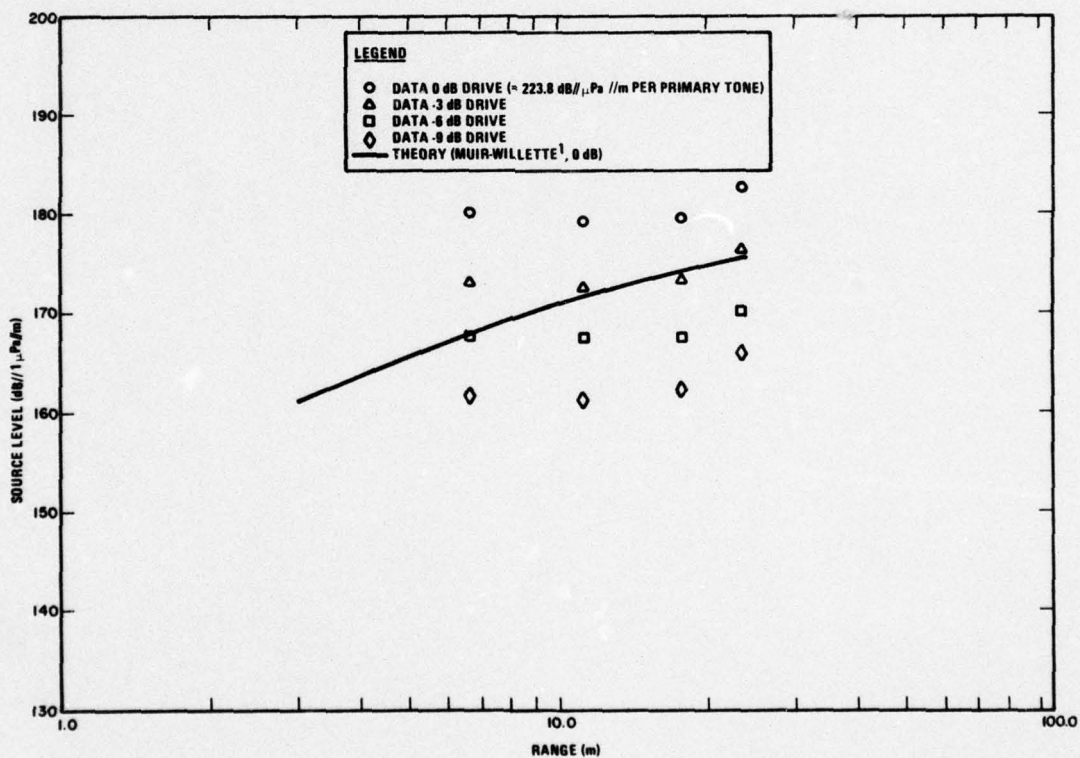


Figure 2-3. Secondary Frequency Source Level at 1.5 kHz as Measured for Four Drive Levels (Seneca Lake Experiment)

3.0 CORRECTION OF DATA

Because all of the data from the two experiments contain some amount of distortion, a method was sought to estimate the amount of error caused by the distortion and to perhaps correct the data. In order to do this, it was necessary to place some reliance on a theoretical model. However, this reliance was kept to a minimum by assuming that the theoretically derived levels for the two shortest range points had the correct ratio (difference in dB). Reliance on derived absolute levels was therefore avoided. The resulting corrected level for the shorter of the two ranges used is highly dependent on the theoretical ratio used. The other corrected values are quite insensitive to the assumed ratio, becoming less so as the range is increased.

The following assumptions were used in the correction procedure:

- 1) The measured pressure p_m is the sum of a signal pressure p_s and interference pressure p_I .
- 2) The interference pressure is proportional to the square of the primary pressure. The primary pressure is inversely proportional to range except in the nearfield. For nearfield points, the spherical wave correction given by Bobber¹⁰ is used. With the nearfield correction expressed as a linear factor denoted by δ , the interference pressure may be written

$$p_I = p_{I0} \delta^2 / r^2$$

Note that δ varies between 0 and 1, assuming the unity value in the farfield of the projector.

- 3) The signal levels at the two lowest ranges are proportional to the theoretical levels at those ranges, i. e., if p_{s1} and p_{s2} are the signal levels and p_{t1} and p_{t2} are the corresponding theoretical levels then

$$p_{s2} = \frac{p_{t2}}{p_{t1}} p_{s1}$$

The two lowest ranges are used because they contain the greatest proportion of interference and hence the least sensitivity to the actual signal level in estimating the interference pressure.

With the above assumptions, a system of equations may be written. At range 1 (eg. 3.0m) the measured pressure is written

$$p_{m1} = p_{s1} + p_{I0} \delta_1^2 / r_1^2$$

At range 2 (eg. 6.0m), the measured pressure is written using assumption 3 above,

$$p_{m2} = p_{s1} \frac{p_{t2}}{p_{t1}} + p_{I0} \delta_2^2 / r_2^2.$$

For each frequency, the above equations can be solved for p_{I0} , which is then used to correct the data at all ranges. The only nearfield range point considered is the 3.0m point in the TRANSDEC experiment, for which the value of δ_1 , is 0.8224. In all other cases, $\delta_1 = \delta_2 = 0$. The Lockwood⁵ model was used to provide the theoretical ratio.

4.0 EXPERIMENTAL RESULTS

The experimental data obtained at TRANSDEC are plotted in Figures 4-1 through 4-10. In each figure the measured data are shown as solid circles. The solid line represents theory calculated using Lockwood's model⁵ and the dashed line represents theory calculated from the Muir-Willette¹ model. The crosses represent corrected data, calculated assuming that the Lockwood theory has the correct short range slope.

The two theories are shown because they demonstrate the contrast between the results of different types of approximations. Other theories are compared in the next section. At the larger ranges it would be initially expected that the Muir-Willette model would be more correct than the Lockwood model because of the explicit inclusion of the primary frequency beam pattern. However, for reasons discussed in the next section, the Muir-Willette results may be as much as 1.0 dB conservative. The Lockwood model is expected to be more correct at ranges below 6.0 m because of the inclusion of a planewave nearfield.

The source levels used in the TRANSDEC experiments were easily low enough to make finite-amplitude attenuation negligible. Under such conditions, the secondary pressure increases as the square of the primary pressure and for every 1.0 dB of increase in the mean primary source level the secondary source level increases 2.0 dB. For convenience the theoretical data were all calculated using a mean primary frequency source level of 227.8 dB// μ Pa/m, and the measured data shown in Figures 4-1 through 4-10 have been scaled up by twice the source level difference. The amounts by which the levels at each frequency have been increased are shown in Table 4-1. In a few cases more than one data value was obtained. These generally agreed within about 1.0 dB and are shown here as average values.

There is a considerable variability in which theory best fits the data. When there is a theoretical discrepancy of 2.0 dB it is difficult to resolve even by distortion free measurements because of the quadratic dependence on the primary source level. The test facilities are considered to have accuracies of about ± 1.0 dB and a 1.0 dB error in estimating the primary frequency source level leads to a 2.0 dB error in the secondary level. In any case, Figure 4-1 shows corrected data that are very close to the dashed Muir-Willette¹ curve, the solid Lockwood⁵ curve being higher. In Figure 4-2, the 12 m data point is not really consistent but otherwise the Muir-Willette theory is favored. In Figure 4-3, the 3.0 m point was discarded because it led to unreasonable corrected levels. The remaining points tend to agree with the dashed line. In Figure 4-4, the solid line is favored. The data in Figure 4-5 also favor the Lockwood curve. Figure 4-6 does not really favor either curve. It appears that in this case, the correction procedure resulted in too high a distortion level. In Figures 4-7 through 4-10 the trend is toward data that support both theories equally well.

The data obtained at Seneca Lake are shown in Figures 4-11 through 4-13. Here, data were obtained at only three frequencies. The primary source level was a constant 233.8 dB// μ P/m per tone, still too low for significant finite-amplitude effects at these ranges. The minimum range for these data was 6.74 m, limited by the test configuration. There is a general tendency for these data to be high. They give a reasonable fit to the solid curves, but are significantly higher than the dashed curves.

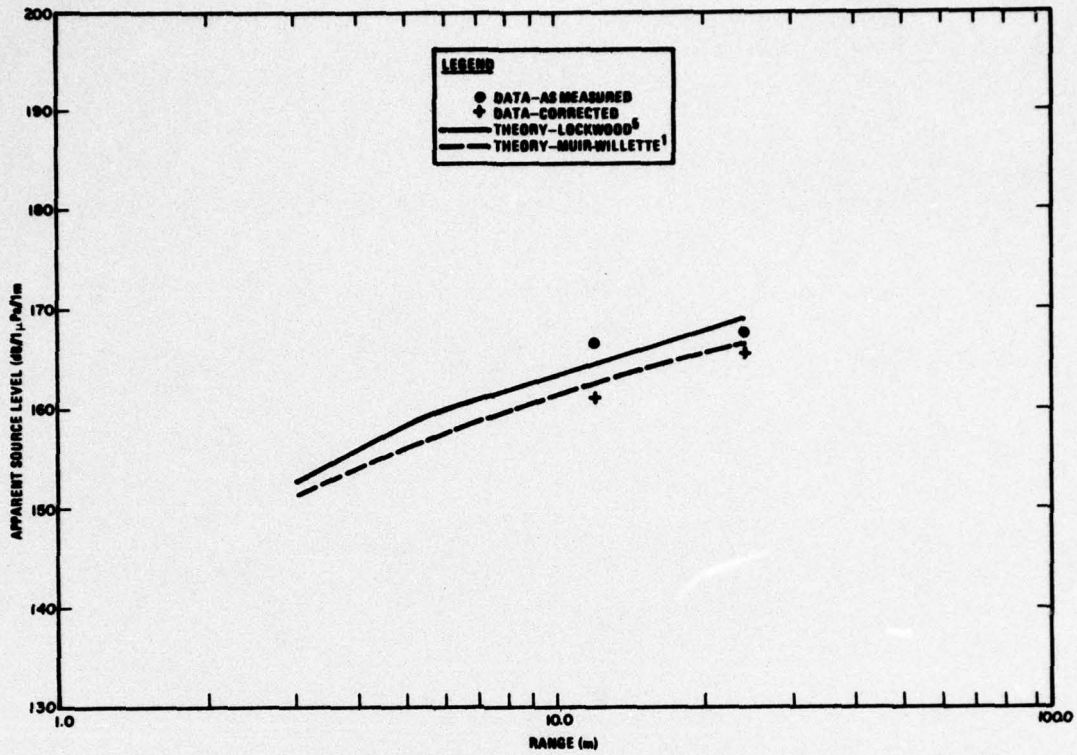


Figure 4-1. TRANSDEC Data at 1.0 kHz Difference Frequency

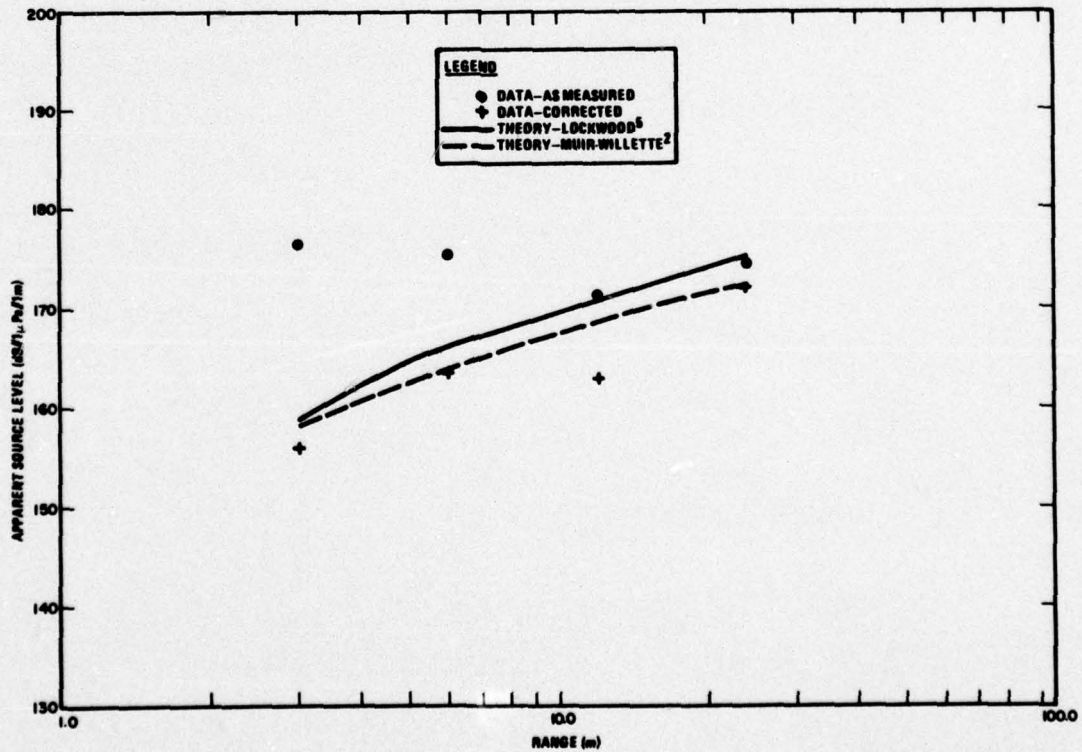


Figure 4-2. TRANSDEC Data at 1.5 kHz Difference Frequency

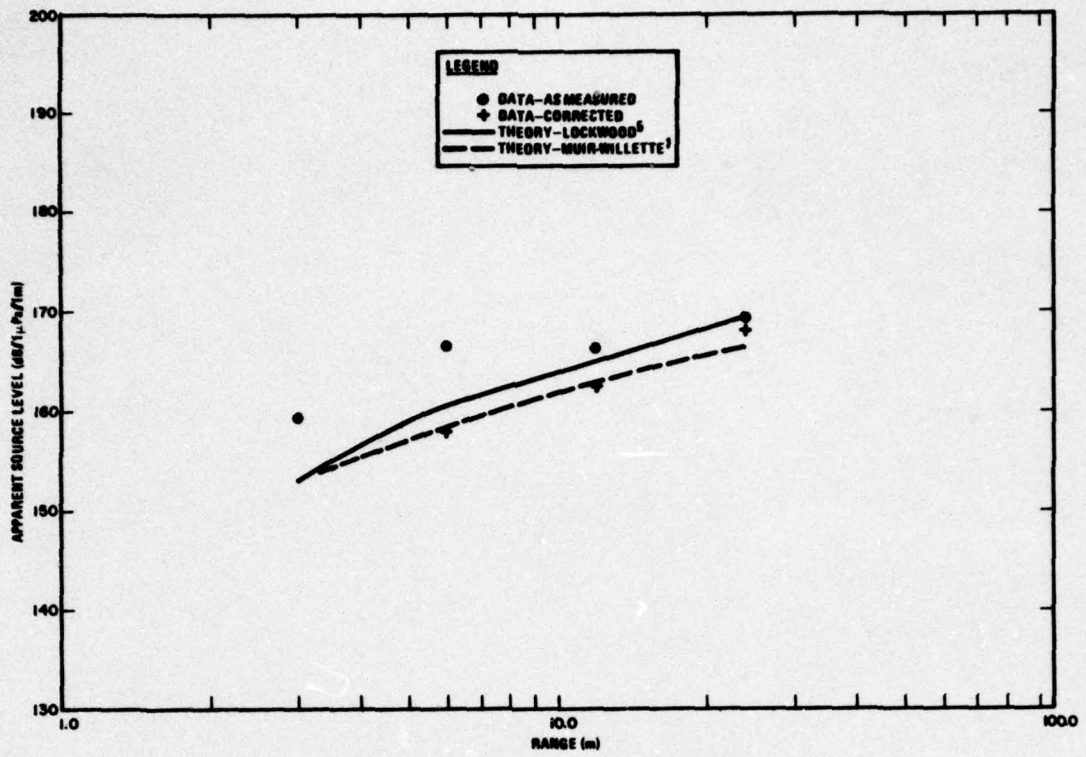


Figure 4-3. TRANSDEC Data at 2.0 kHz Difference Frequency

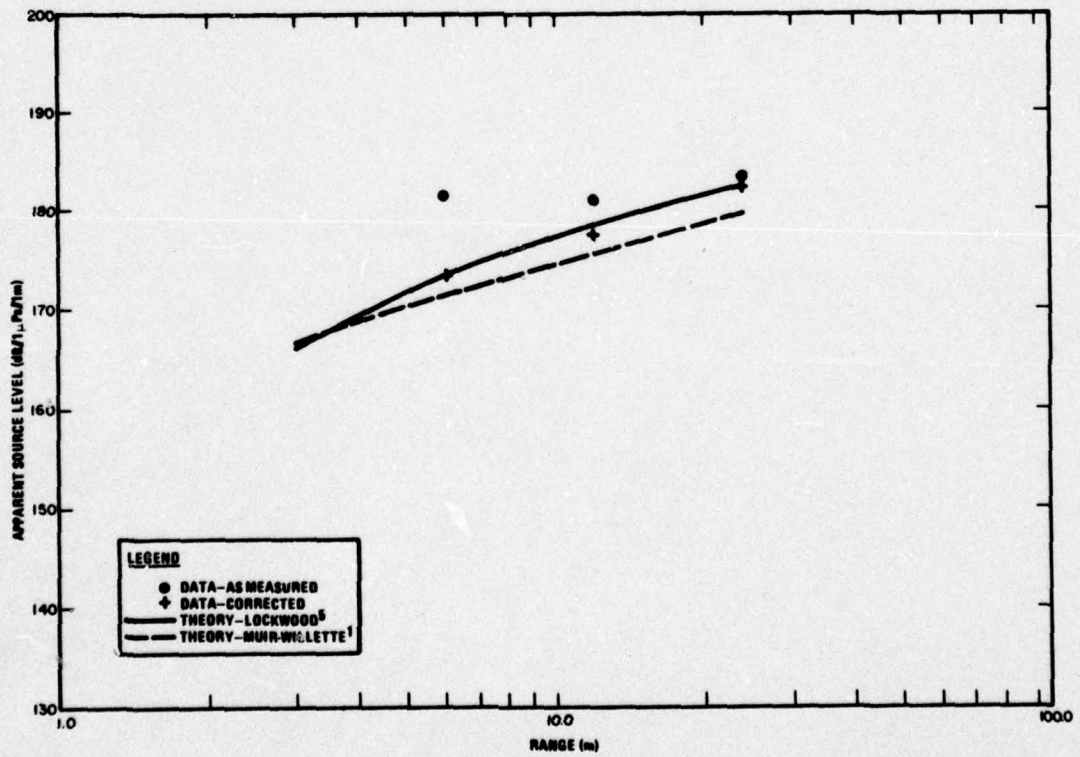


Figure 4-4. TRANSDEC Data at 2.5 kHz Difference Frequency

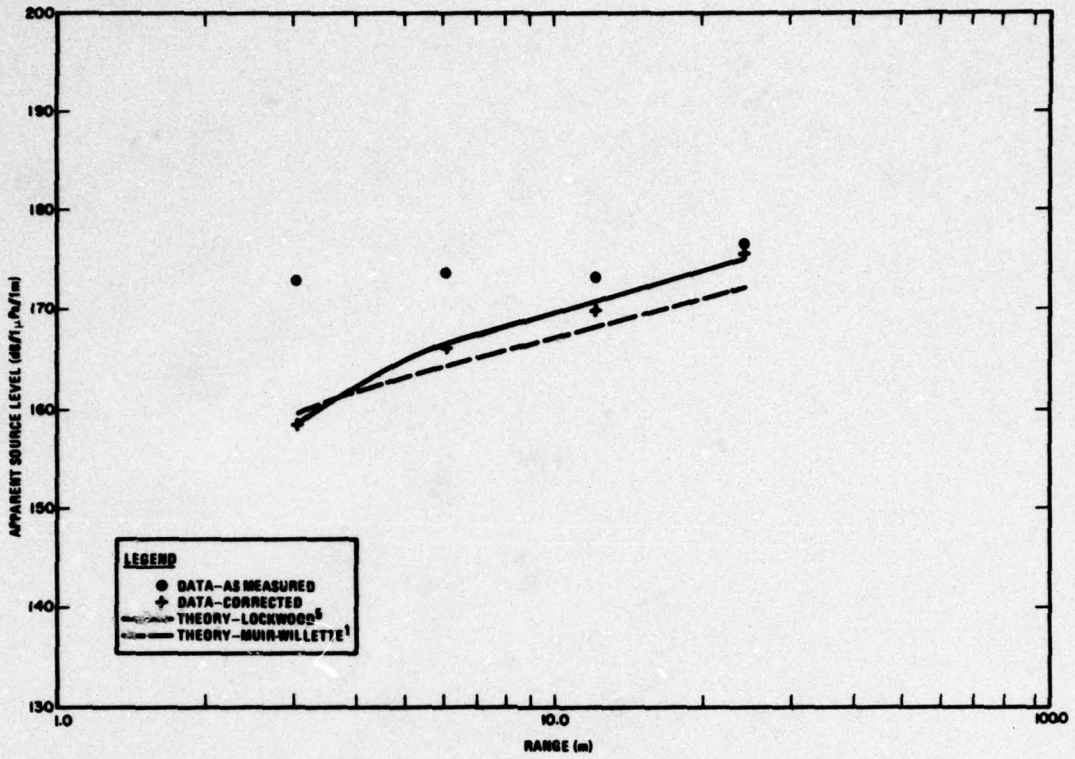


Figure 4-5. TRANSDEC Data at 3.0 kHz Difference Frequency

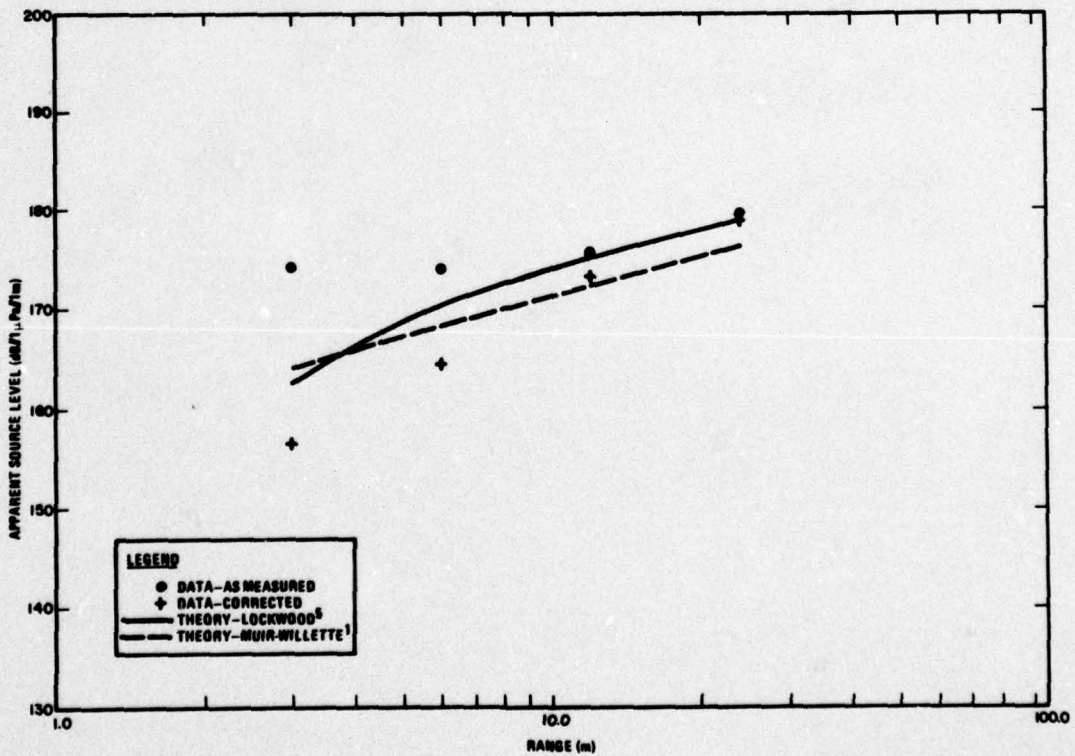


Figure 4-6. TRANSDEC Data at 4.0 kHz Difference Frequency

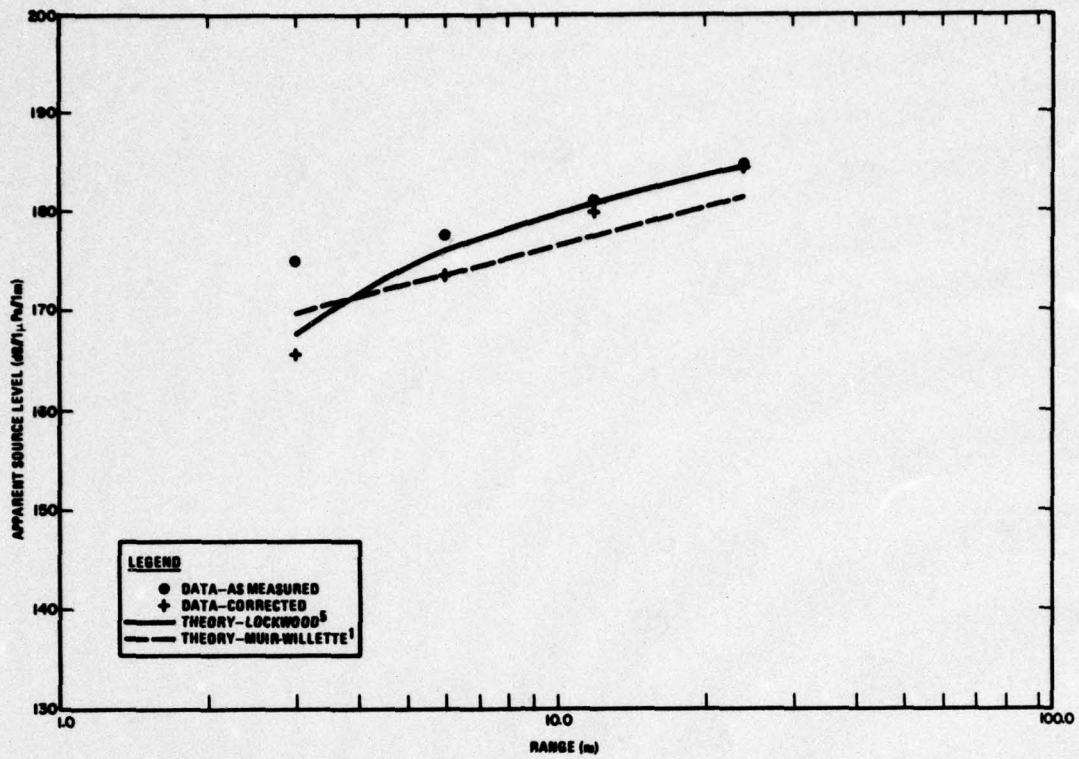


Figure 4-7. TRANSDEC Data at 6.0 kHz Difference Frequency

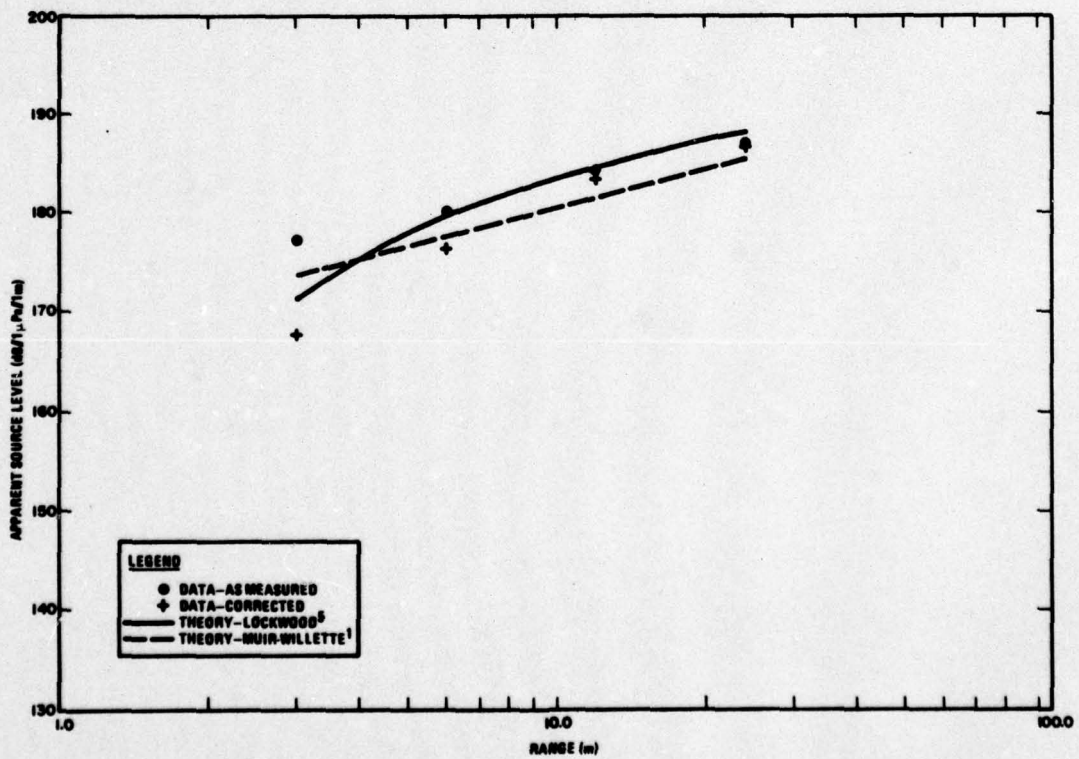


Figure 4-8. TRANSDEC Data at 8.0 kHz Difference Frequency

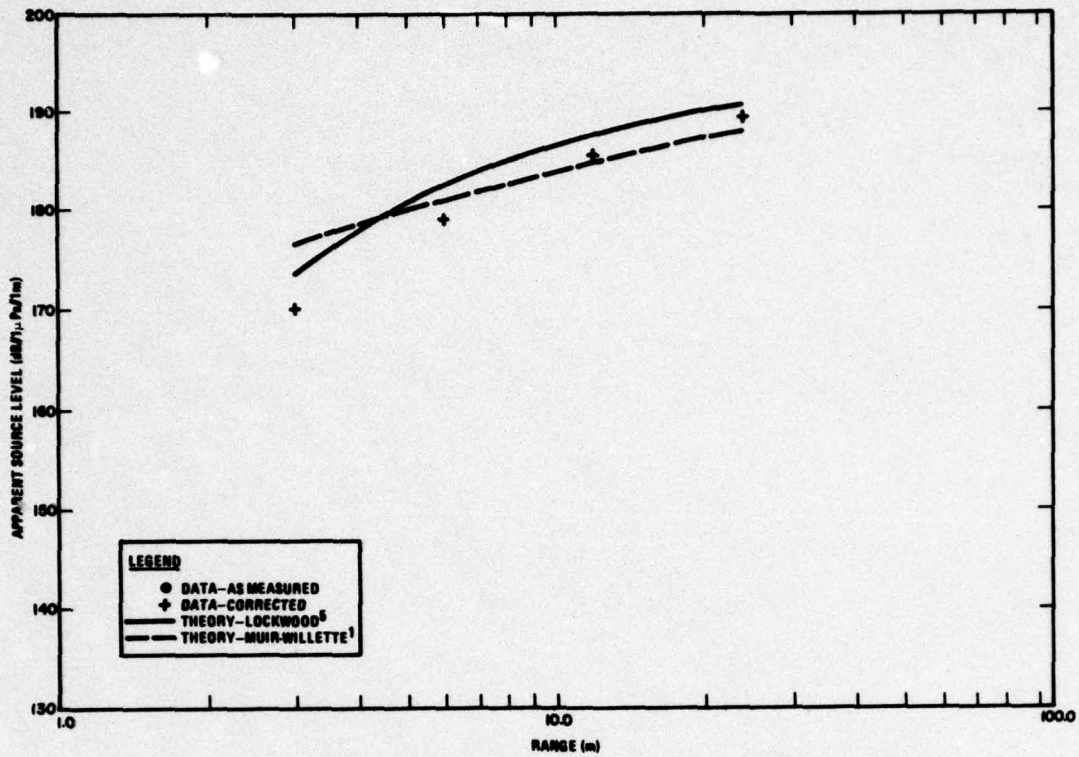


Figure 4-9. TRANSDEC Data at 10.0 kHz Difference Frequency

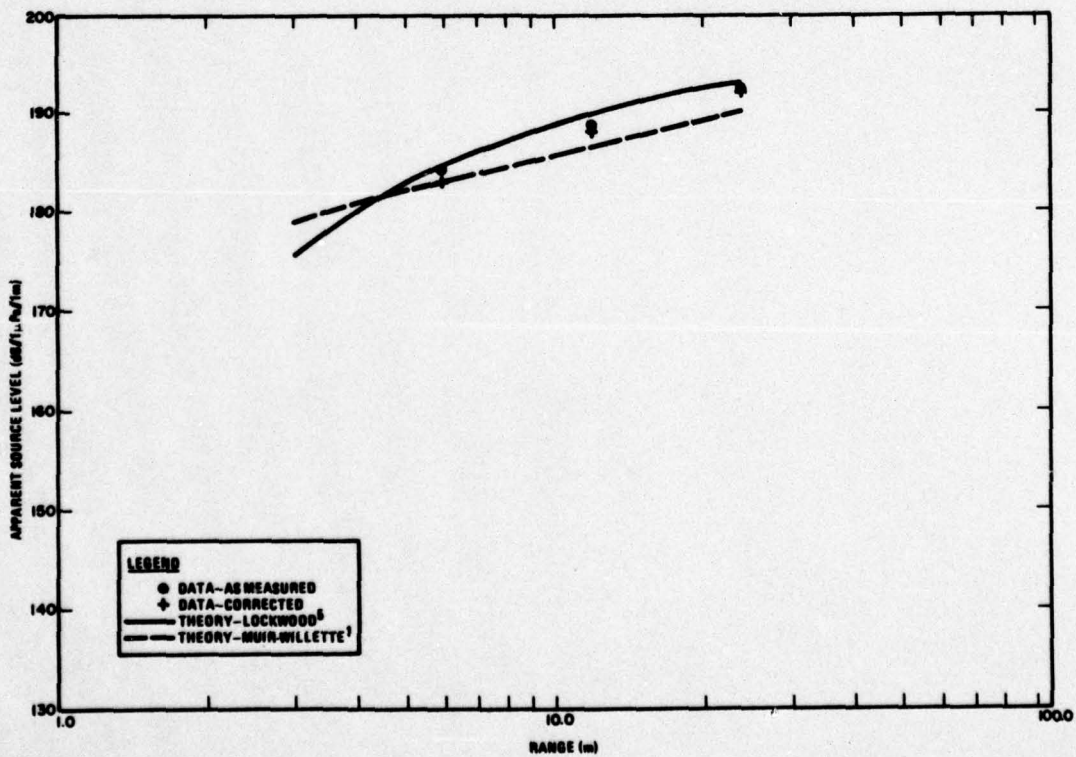


Figure 4-10. TRANSDEC Data at 12.0 kHz Difference Frequency

Table 4-1. Measured Data Increases to Compensate for Assumed Constant Mean Source Level

Difference Frequency	Correction (dB)
1.0	2.2
1.5	1.8
2.0	1.6
2.5	1.6
3.0	1.9
4.0	1.9
6.0	4.6
8.0	6.0
10.0	7.5
12.0	8.1

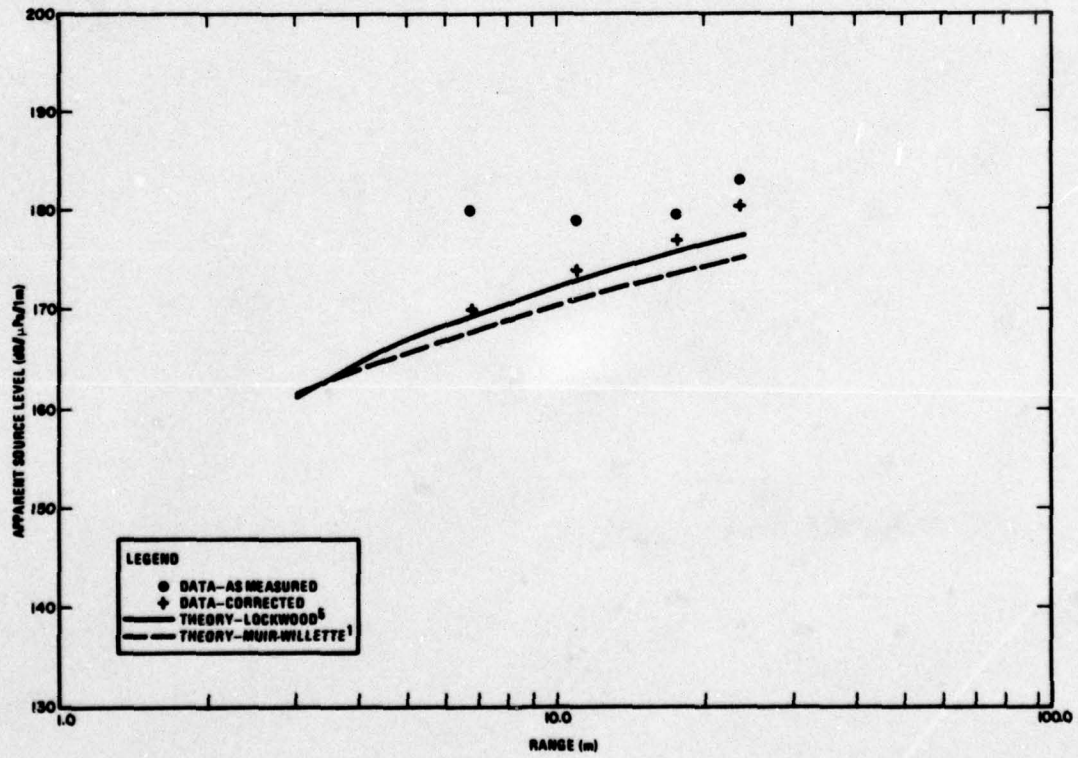


Figure 4-11. Seneca Lake Data at 1.5 kHz Difference Frequency

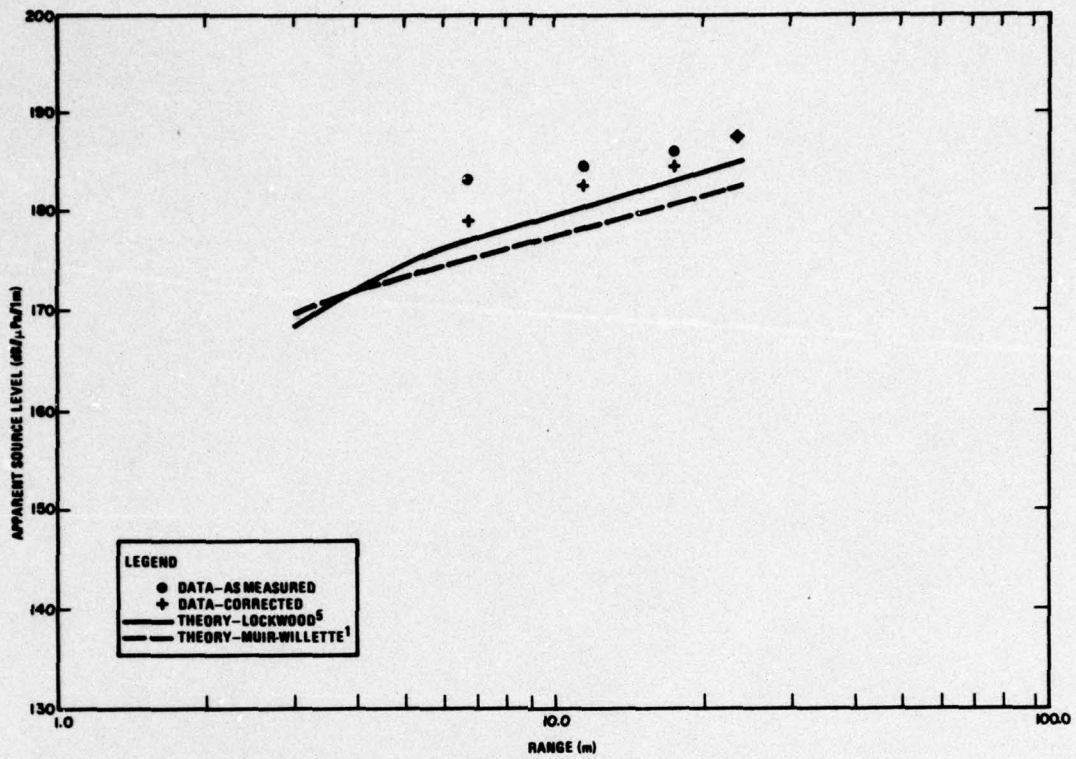


Figure 4-12. Seneca Lake Data at 2.5 kHz Difference Frequency

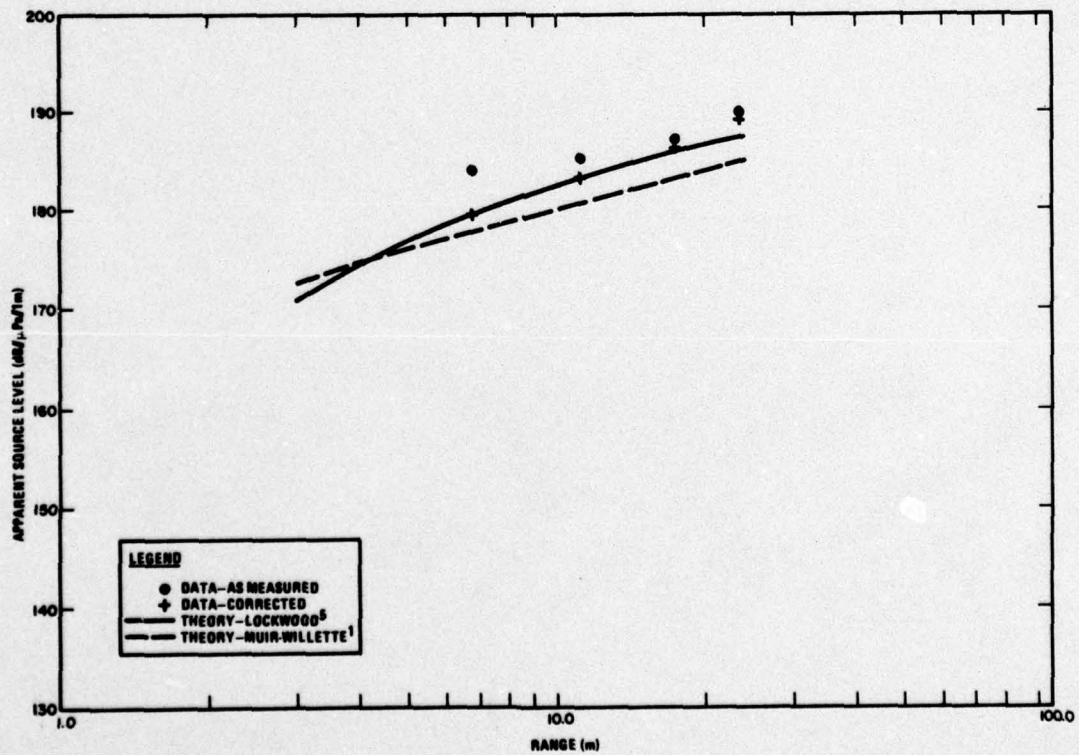


Figure 4-13. Seneca Lake Data at 3.0 kHz Difference Frequency

5.0 COMPARISON OF THEORETICAL RESULTS

A convenient way of looking at the parametric array nearfield has the interaction volume divided into apertures formed by slicing the primary beam perpendicular to its acoustic axis. Each such aperture radiates secondary signals with a farfield level that depends on the amplitude and phase distribution of the source strength density in the aperture and on the distance from the aperture to the measurement point. Each aperture also has a nearfield. The amplitude and phase at a measurement point is the sum of the signals from all of the apertures from the projector out to the measurement point.

The accuracy of any nearfield model, assuming that loss mechanisms may be neglected, depends on the accuracy with which the primary field is modeled and on the accuracy with which the contributions of all the virtual sources are summed at the measurement point. Most of the nearfield models that have been proposed treat the primary beam as a spherically spreading wave retaining the assumed farfield characteristics all the way back to the source. The exceptions are the strictly cylindrical-beam models such as those of Berklay³ and of Mellen⁸, and Lockwood's model⁵, which combines a planewave nearfield and a spherically spreading farfield. The conical beam models are not applicable to measurement points in the primary beam's nearfield. Another issue concerning the description of the primary beam is the assumed beampattern. In the models of Bartram⁴, Mellen⁸ and Lockwood⁵, the farfield beam is assumed to be conical, with equal amplitude over a spherical cap, and with energy equal to the total radiated energy. A description that is, in principle, more precise incorporates the theoretical beampattern of the projector. The Muir-Willette¹, Rolfeigh⁷ and the new Mellen-Moffett⁹ nearfield models are examples of this type of treatment. It turns out that there is generally a discrepancy of about 2.0 dB for cases considered in the present work between models incorporating the primary beampattern and those not. This is because the major lobe of the circular piston pattern accounts for only about 80% of the radiated energy. While the assumption that 100% of the primary frequency energy contributes to the secondary source strength clearly represents an upper bound, the models that incorporate the beampattern tend to be conservative for two reasons. First, they all assume that the primary beampattern applies all the way back to the source. It seems reasonable to expect 100% of the primary frequency energy to contribute in the projector nearfield because the sidelobe energy is still in the column. The second reason is that it is usual to assume that negligible signal comes from outside the major lobe. In the Muir-Willette model¹, for example, the integration over angle is only carried out to the first null of the primary pattern. Yet, in nearfield cases, energy from the sidelobes may be significant. A preliminary test of the Muir-Willette model in which the angle included in the integration was quadrupled showed an increase of about 0.3 dB for cases of present interest. From the two reasons combined, the models may well be low by as much as 1.0 dB at 24.0 m and even more at shorter ranges that are still in the projector farfield.

There are two significant issues related to the accuracy with which the contributions of all of the virtual sources are summed at the measurement point. The most basic consideration is that the variation of the range from the measurement point to each virtual aperture be

accounted for. All nearfield models do this. The other issue is the handling of the apertures for which the measurement point is in the nearfield. Because of their proximity to the measurement point, phase varies rapidly over these apertures, and care should be taken to see that they are properly described. The accuracy of the various models in this regard and the quantitative effect of errors are difficult to assess.

Six of the theories discussed above have been evaluated for the conditions of the Seneca Lake experiment. The results for frequencies of 1.5, 3.0 and 10.0 kHz are shown in Figures 5-1 through 5-3. The theories represented by lines are those of Bartram⁴, Rolleigh, Lockwood⁵, Muir and Willette¹, and Mellen⁸ (cylindrical and conical versions). Because of the assumptions of a conical primary beam, none of the theories shown are expected to be valid within 6.0 m except for the Mellen⁸ cylindrical model and the Lockwood⁵ model. These two models are in reasonable agreement between 3.0 and 6.0 m, although the Lockwood model appears to be relatively low at the 10 kHz frequency. If one discounts the Mellen cylindrical model beyond 6.0 m, then all of the theoretical results fall within about 3.0 dB at 1.5 kHz, 3.5 dB at 3.0 kHz and 4.5 dB at 10.0 kHz. The increase in spread appears to be attributable solely to a drop in the Muir-Willette¹ curve relative to the others. However, on close inspection, it is observed that the Muir-Willette¹ and Lockwood⁵ theories appear to retain a constant ratio as frequency is varied. Also, the Bartram⁴ and Rolleigh⁷ theories tend to keep the same ratio but to change relative to the Muir-Willette and Lockwood theories. The Mellen⁸ (conical) curve does not seem to consistently track either of the pairs of theoretical curves mentioned above.

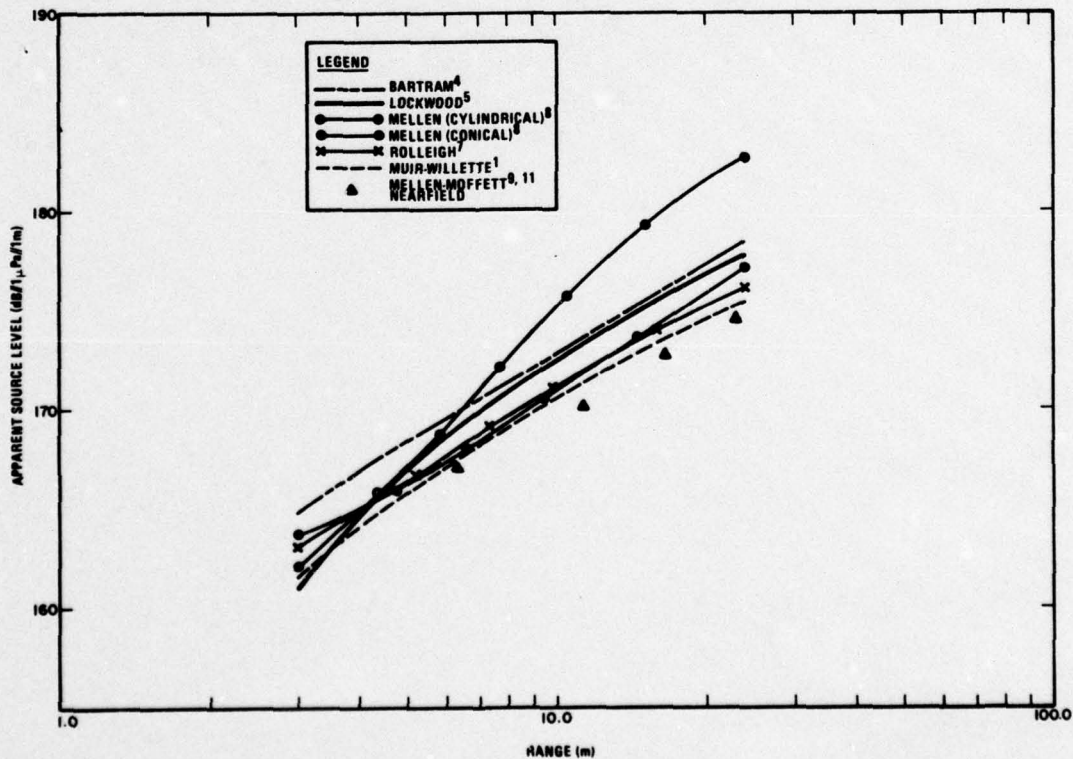


Figure 5-1. Comparison of Theoretical Data for 1.5 kHz Difference Frequency (Conditions of Seneca Lake Experiment Assumed)

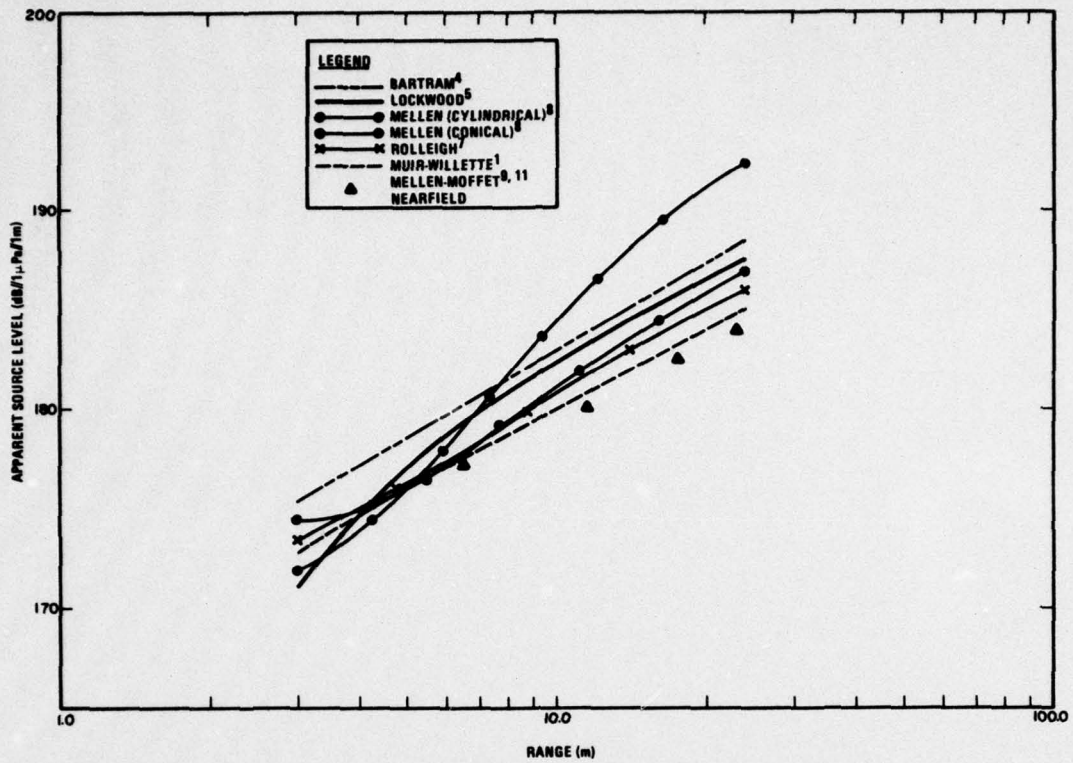


Figure 5-2. Comparison of Theoretical Data for 3.0 kHz Difference Frequency (Conditions of Seneca Lake Experiment Assumed)

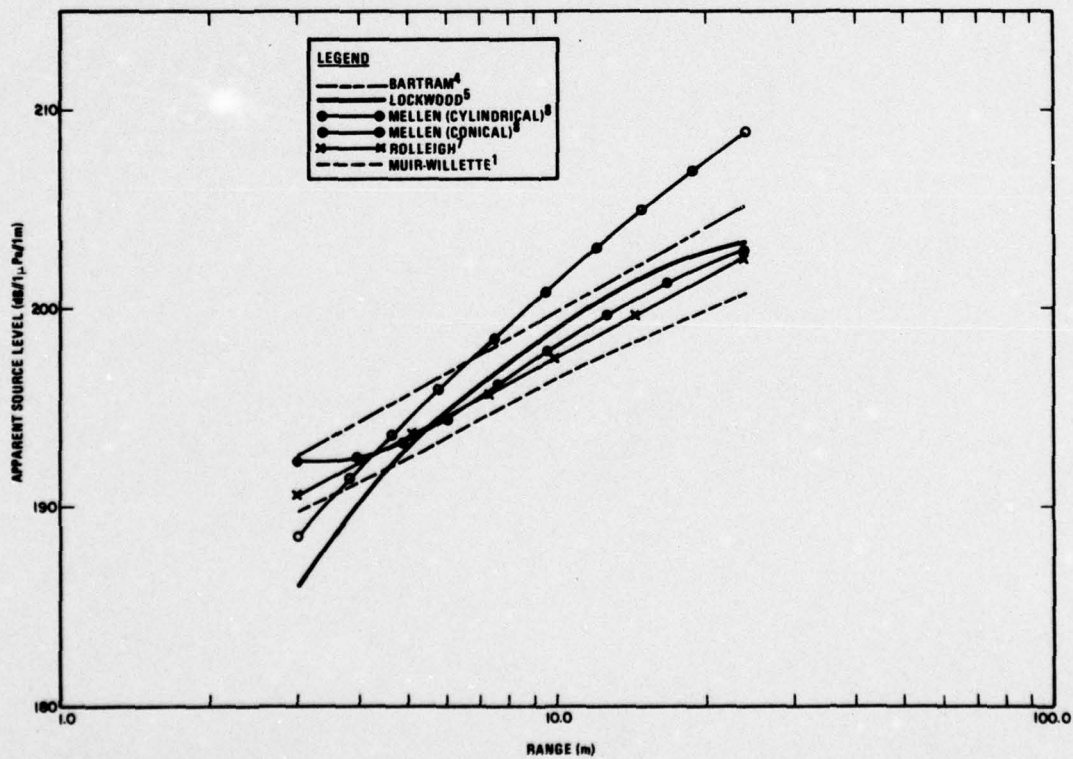


Figure 5-3. Comparison of Theoretical Data for 10.0 kHz Difference Frequency (Conditions of Seneca Lake Experiment Assumed)

The reason for this shift with frequency of two theories relative to two others is not fully understood, but is believed to be related to the method of handling the apertures that are in the nearfield relative to the observation point. The shift at short ranges of the Mellen (cylindrical) theory relative to the Lockwood theory may also be related to the handling of nearfield apertures.

The offset between the Bartram⁴ and Rolleigh⁷ theories and between the Lockwood⁵ and Muir-Willette¹ theories at ranges greater than the projector's nearfield distance is believed to be caused by the explicit account of the primary frequency beampattern in the Rolleigh and Muir-Willette models. In each case, the offset is about 2.0 dB. It is interesting to note that 2.0 dB is the approximate ratio of the total radiated energy to the energy in the main lobe for the projector considered. The Bartram and Lockwood models assume that all of the radiated energy goes into the interaction, whereas the models that incorporate a beampattern include little that is not in the major lobe. A 2.0 dB discrepancy is therefore consistent with this fact.

Although the inclusion of the beampattern is, in principle, more accurate than the simpler model, in practice, the results tend to be conservative. This is largely because of the use of the approximation that the primary beam is conical all the way to the origin. In the primary nearfield, it seems reasonable to expect all of the energy to contribute to the secondary signal, not just the 80% in the major lobe. In fact, it might be argued that all energy within the first Fresnel zone relative to the observation point should contribute. A further effect of using the theoretical beampattern that may lead to erroneous results is the non-ideal nature of the primary frequency beampattern. High sidelobe levels may increase the amount of energy contributing to the axial secondary signal. For conditions of the present experiments, the explicit inclusion of the primary frequency beampattern combined with the conical beam assumption is estimated to lead to results that are too low by a minimum of 0.5 dB at 24.0 m. An error of as much as 1.0 dB is not unlikely. Therefore, it appears that if two models were precisely correct in all respects except the handling of the primary beampattern, then the version with the theoretical beampattern included should provide a lower bound, the model assuming all radiated energy to occupy a constant amplitude cone should provide an upper bound, and the "true" value should lie in the middle.

In summary, all models considered are within 3.0 dB in their regions of applicability at 1.5 kHz. The spread among the results increase as frequency is increased, with the Bartram and Rolleigh data maintaining an approximately constant ratio and the Lockwood and Muir-Willette data maintaining an approximately constant ratio. In each case, the constant ratio is approximately 2.0 dB and can be attributed to the handling of the primary beampattern. The disparity between the Bartram and Rolleigh models on one hand and the Lockwood and Muir-Willette models on the other is unexplained, but is believed related to the handling of geometry close to the measurement point.

The data represented by triangular points on Figures 5-1 and 5-2 have been left for discussion at the end of the section because they were not evaluated by the present author and are not available at the entire span of ranges and frequencies considered. These data were supplied by Moffett¹¹ using parameters supplied by the author for the conditions of the Seneca Lake experiment. These data from the new Mellen-Moffett⁹ nearfield model agree quite well with the Muir-Willette¹ results, but tend to be lower, in some cases by as much as 1.0 dB.

6.0 CONCLUSIONS

Results from two parametric nearfield experiments have been reported. The data, known to contain substantial receiving hydrophone intermodulation distortion, have been corrected by deducing the level of the distortion and coherently subtracting the distortion pressure from the measured data. The data obtained at TRANSDEC at ten frequencies support both the Lockwood⁵ and the Muir-Willette¹ theories quite well. Note that the latter is not considered valid at ranges less than 6.0 m; so any disagreement in this region is disregarded. Because the data seem to support both theories equally well, they especially support the contention that the two theories are, respectively, upper and lower bounds. Comparison with other theories considered may be effected indirectly by referring to Figures 5-1 through 5-3. Although the figures were prepared for the conditions of the Seneca Lake experiment, the comparison of relative levels for a given frequency is equally applicable to the TRANSDEC experiment conditions.

When the theories are compared in light of the TRANSDEC data, it appears that the Bartram⁴ theory has a tendency to be high. The Rolleigh⁷ and Mellen⁸ (conical) theories, in the primary farfield where they are valid, tend to lie between the Lockwood⁵ and Muir-Willette¹ curves and so agree well with the experimental data. The fact that these models tend to shift with frequency relative to the Lockwood and Muir-Willette curves is somewhat disturbing.

The Seneca Lake data tend to be somewhat high relative to the Muir-Willette and Lockwood curves, giving a reasonable fit only to the latter. However, the conditions under which these data were obtained are such that little confidence can be associated with them.

A test of several nearfield theories has been made. Because of the condition of the experimental data, the test is not particularly discriminating. Also, there is not a great deal of spread among the theories considered. Within their regions of validity, the theories of Rolleigh⁷, Mellen⁸, Muir and Willette¹ and Lockwood⁵ all give good agreement with experiment. Of these, the last is the only one that is uniformly valid at points in both the nearfield and farfield of the projector.

In conclusion, it is of interest to compare the difficulty of applying the various models considered. Table 6-1 gives for each model the degree of difficulty on a scale of 1 (easy) to 10 and the minimum equipment requirement for evaluation.

Table 6-1. Degree of Difficulty and Equipment Required for Each Model

Model	Difficulty	Equipment Required
Bartram ⁴	1	Slide Rule
Mellen ⁸	2	Slide Rule
Lockwood ⁵	3	Programmable Calculator
Muir-Willette ¹	10	Large Computer
Rolleigh ⁷	1	Slide Rule
Mellen-Moffett Nearfield ⁹	10	Large Computer

7.0 LIST OF REFERENCES

1. T.G. Muir and J.G. Willette, "Parametric Acoustic Transmitting Arrays," *J. Acous. Soc. Am.* 52, 1481 (1972).
2. T.G. Muir, L.L. Mellenbruch and J.C. Lockwood, "Reflection of Finite-Amplitude Waves in a Parametric Array," *J. Acous. Soc. Am.* publication pending.
3. H.O. Berkday, "Nearfield Effects in Parametric End-Fire Arrays," *J. Sound Vib.* 20, 135 - 143 (1972).
4. J.F. Bartram and R.P. Fugitt, "Nearfield Effects in a Parametric Transmitting Array," 87th Meeting of the Acoustical Society of America, New York, April 1974.
5. J.C. Lockwood and D.P. Smith, "Investigation of the Increase in Parametric Efficiency Due to Bubbles," Final Report under Contract N00024-74-C-1151, AMETEK, Straza Div., El Cajon, CA, August 1974.
6. R.H. Mellen and M.B. Moffett, "A Model for Parametric Sonar Radiator Design," Naval Underwater Systems Center, Technical Memorandum No. PA4-229-71 (Sept. 1971).
7. R.L. Rolleigh, "Difference Frequency Pressure Within the Interaction Region of a Parametric Array," *J. Acous. Soc. Am.* 58, 964 -971 (1975).
8. R.H. Mellen, "A Nearfield Model of the Parametric Radiator," Naval Underwater Systems Center, Technical Memorandum No. PA4-230.75, December 1975.
9. R.H. Mellen and M.B. Moffett, "Numerical Method for Calculating the Nearfield of a Parametric Acoustic Source," *J. Acous. Soc. Am.* 61, S83 (A) (1977).
10. R.J. Bobber, Underwater Electroacoustic Measurements (U.S. Government Printing Office, Washington, D.C. 1970).
11. M.B. Moffett, Private Communication, June 1977.

APPENDIX A

In this appendix is supplied for reference a FORTRAN listing of the main program and required subprograms used to evaluate the Muir-Willette model. The original model is described in Reference 1. Modifications made by the author are noted in the comments at the beginning of the listing.

```

1  C PROGRAM WILLET(INPUT,OUTPUT)
    C THIS PROGRAM COMPUTES THE AXIAL SOURCE LEVEL OF A PARAMETRIC
    C ARRAY BY THE VOLUME INTEGRATION METHOD. THE PROGRAM WAS
    C ORIGINALLY WRITTEN BY J. G. WILLETTE AT APPLIED RESEARCH
    C LABORATORIES, THE UNIVERSITY OF TEXAS AT AUSTIN. SUBSTANTIAL
    C MODIFICATIONS WERE SUBSEQUENTLY MADE BY J. C. LOCKWOOD.
    C THESE MODIFICATIONS INCLUDE 1) THE INCLUSION OF A FINITE
    C AMPLITUDE TAPER FUNCTION, 2) REVISION OF THE INPUT PARAMETERS
    C TO SI UNITS, AND 3) APPLYING A SINH STRETCHING TO THE RANGE
    C VARIABLE TO REDUCE THE NUMBER OF INTEGRATION STEPS REQUIRED
    C FOR CONVERGENCE.
10  C
15  C PROGRAM INPUT REQUIRES THREE CARD TYPES. CARD TYPE 1 IS IN
    C (BE10.3) FORMAT AND REQUIRES FK1 AND FK2, TWO PRIMARY
    C FREQUENCIES IN HZ, P1 AND P2, TWO RMS PRIMARY SOURCE LEVELS
    C IN DB RE 1 MICROPASCAL AT 1 M, A, PISTON RADIUS IN METERS,
    C TEMP, WATER TEMPERATURE IN DEGRES CELSIUS, AND S, SALINITY
    C IN PARTS PER THOUSAND.
20  C CARD TYPE 2 IS IN FORMAT (2I10,2F10.0) AND REQUIRES IJ, A
    C CONVERGENCE TEST CONTROL, M, THE RANGE INTEGRATION STEP
    C CONTROL, XNM, THE AZIMUTH INTEGRATION STEP CONTROL, AND
    C BOVERA, THE PARAMETER OF NONLINEARITY, AND DEPTH THE
    C PROJECTOR DEPTH IN METERS. IJ TAKES THE VALUES
    C 1 AND 2. IF IT IS 1, A CONVERGENCE TEST IS PERFORMED WHICH
    C CONSISTS OF ADDING 10 TO THE NUMBER OF RANGE INTEGRATION STEPS
    C AND RECOMPUTING SLD. THE DIFFERENCE IS OUTPUT AS DELTA AND IS
    C A MEASURE OF THE CONVERGENCE. M IS THE NUMBER OF STEPS IN THE
    C RANGE INTEGRATION. XNM IS THE NUMBER OF AZIMUTH STEPS PER
    C DEGREE OF MAIN LOBE HALFWIDTH. THE INTEGRATION IS CARRIED OUT
    C BETWEEN THE FIRST INFINITIES OF THE PRIMARY BEAM MAIN LOBE.
30  C
    C CARD TYPE 3 IS OF FORMAT (E10.3) AND REQUIRES A RANGE IN METERS.
35  C A ZERO VALUE FOR FK1 ON CARD TYPE ONE TERMINATES THE PROGRAM.
    C OTHERWISE, CARD TYPE 1 IS ALWAYS FOLLOWED BY ONE CARD TYPE 2.
    C THEN, AS MANY CARDS TYPE 3 AS DESIRED ARE INPUT. A ZERO
    C RANGE SIGNALS A NEW CASE, AND A NEW CARD TYPE 1 IS READ.
40  C
    C J. C. LOCKWOOD
    C 17 MAY 1977
45  C COMMON ATPA2,BK1(400),COSX(400),SINX(400),R,KD,IFSH,ITIME,OUTR(200CTH00010
    C *D),OUTI(2000),RO,A,K1,K2,RMAX,ALPHAD,P1,P2,BOVERA,SHRD,SIG,CG , CTHC00?3
    C 1RFL,XYZ,ZU
    C DIMENSION X(34)
    C REAL K1,K2,KD
    C REAL JO,J1
    C DATA X/4HWD ,4H ,4HSM R,4HD ,4HP1 ,4H ,4HK1 ,4H
    C *4HK2 ,4H ,4HA ,4H ,4HRH0D,4H ,4HCD ,4H ,4HB/A
    C *4H ,4HHWD,4HTH ,4HKD ,4H ,4HALPH,4HA1 ,4HALPH,4HA2 ,
    C *4HP2 ,4H ,4HALPH,4HAD ,4HF1 ,4H ,4HF2 ,4H /
    C ASINH(X)=ALOG(X+(X*X+1)**.5)
    C PI=3.141592 $ TUPI=2.0*PI
    C THE FOLLOWING STATEMENT READS CARD TYPE 1
55  C READ 2,FK1,FK2,P1,P2,A,RH00,TEMP,S
    C IF(FK1.EQ.0.0)GO TO 12
    C P1=PI-96.2227

```

```

CTH00070
CTH00080
CTH00100
CTH00110
CTH00120
CTH00130
CTH00140
CTH00160
CTH00190
CTH00220

```

```

P2=P2-96.2227
A=A+100.
RH00=RH00/1000.
C THE FOLLOWING STATEMENT READS CARD TYPE 2
READ 301,I,J,M,XNN,BOVERA,DEPTH
PRESS=DEPTH*.097+1.
301 FORMAT(2I10,3F10.0)
MM=M
FKD=ABS(FK1-FK2)
WN=TUPI*FKD $ CO=SPEED(S,TEMP,PRESS)
CO=CO $ RMAX=SMRO $ RH00=RH00
K1=TUPI*FK1/CO $ K2=TUPI*FK2/CO
SMRO=(K1+K2)/2.*(A/2.)**2
KD=TUPI*ABS(FK1-FK2)/CO
HWIDTH=ASIN(3.83170571/A/(K1+K2)*2.)/.0174533
ALPHA2=ALF(S,TEMP,FK2/1000.,PRESS)
ALPHA=ALF(S,TEMP,FKD/1000.,PRESS)
401 FORMAT(/,5X,"S = ",F4.1," PPT",5X,"TEMP = ",F5.2," C",5X,/)
REF=91.44
9 FORMAT(*1PARAMETERS (CONVERTED TO CGS ; P1 AND P2 ARE PEAK RE 1 MI
1CROBAR AT 1 YD):",/,(/ ,BX,2A4,2H= ,E16.9))
300 FORMAT(7,9X,2HR ,29X,2MPD,30X,3HSLD,17X,3HDELTA,20X,1HR,/)
PRINT 15
13 FORMAT(/,////)
PRINT 9,X(1),X(2),WD,X(3),X(4),SMRO,X(5),X(6),P1,
?X(27),X(28),P2,X(31),X(32),FK1,X(34),FK2,
?X(7),X(8),K1,X(9),X(10),K2,X(11),X(12),A,X(13),X(14),RH00,
?X(15),X(16),CO,X(17),X(18),BOVERA,X(21),X(22),KD,
?X(23),X(24),ALPHA1,X(25),X(26),ALPHA2,X(29),X(30),ALPHA0,
?X(19),X(20),HWIDTH
PRINT 401,S,TEMP
PRINT 300
1 FORMAT(T115,E10.3)
P1 = 10.0*(P1/20.0)
P2 = 10.0*(P2/20.0)
C=-1.0*WD*WD*REF*REF *P1*P2*(1.0+BOVERA*0.5)
C=C/( 2.0 * RH00*CO**4)
ALPHA2=ALPHA1+ALPHA
ALPHA2=EXP(-ALPHA2)
T=0.0
N=HWIDTH*XNN
J=N/2*28IF(J.NE.N)N=N+1
D = 0.0174533/XNN
NP1=N+1
DO 4 K=1,NP1
COSX(K)=COS(T)
SINX(K)=SIN(T)
IF(SINX(K).NE.0.0)GOTO 31
BK1(K)=BK2 =1.0
60 TO 4
31 CONTINUE
BARG=K1+A*SINX(K) $ BK1(K)=J1(BARG)
BARG=K2+A*SINX(K) $ BK2 =J1(BARG)
BK1(K)=4.0*BK1(K)+BK2 /(K1+K2+A*A*SINX(K))/SINX(K)
T=T+D
4

```

CTH00230
CTH00240
CTH00250
CTHC0260
CTH00280
CTH00290
CTH00300
CTH00310
CTH00320
CTH00330
CTH00360
CTH00380
CTH00390
CTHC0400
CTHC0430
CTHC0440
CTHC0450
CTHC0460
CTHC0470
CTHC0480
CTHC0070
CTH00490
CTH00500
CTH00510
CTH00520
CTH00530
CTH00540
CTH00550
CTH00560
CTH00570
CTH00580
CTH00590
CTHC0600
CTHC0610
CTHC0620
CTHC0630
CTHC0640
CTHC0650
CTHC0660
CTHC0670
CTHC0680
CTHC0690
CTHC0700

```

115 200  FORMAT(1X,20F5.3)
      C 100  THE FOLLOWING STATEMENT READS CARD TYPE 3
120  RO=RO*100.
      IF (RO.EQ.0.) GO TO 999
      M=PI
3  IX1 = IJ
      UMAX=ASINH(RO/2./SMRD)
      XP=R
40  PRINT1,XR
      DELTA=UMAX/XP
      U=0.
      MP1=M+1
      DO 5 L=1,MP1
      P=SMRD*2.*SINH(U)
      IF (L.EQ.MP1) R=RO
      IFSW=1
      ITIME=1
      RADIAN = MWIDTH*0.0174533
      CALL INTEGR(OUTR(L),0.0,RADIAN ,M)
      IFSW=2
      ITIME=1
      CALL INTEGR(OUTI(L),0.0,RADIAN ,N)
      U=U+DELTA
      IFSW=3
      ITIME=1
      CALL INTEGR(AR,0.0,UMAX,P)
      IFSW=4
      ITIME=1
      CALL INTEGR(AI,0.0,UMAX,M)
      AR=AR+C $ AI=AI+C
      AB=SQRT(AR**2+AI**2)
      ADB=20.0*ALOG10(AB)*97.
      IF (IX1.EQ.2) GO TO 8
7  IX1=2
      XLDB=ADB
      GO TO 40
      P=M+10
8  DELTA=(XLDB-ACB)
      YLDB=ADB
      RO=RO/100.
      ADB=ADB+20.*ALOG10(RO)
      PRINT 10,RO,AR,AI,ADB,DELTA
10  FORMAT(2X,E16.9,5X,E16.9,3H + ,E16.9,2H I,5X,E16.9,5X,E16.9)
      GO TO 100
12  PRINT 5252
      FORMAT(1H1)
      END

```

CTH00710
CTH00720
CTH00730
CTH00740
CTH00750
CTH00760
CTH00770
CTH00780

CTH00800
CTH00810
CTH00820
CTH00830
CTH00840
CTH00850
CTH00860
CTH00870
CTH00880
CTH00890
CTH00900
CTH00910
CTH00920
CTH00930
CTH00940
CTH00950
CTH00960
CTH00970
CTH00980
CTH00990
CTH01000
CTH01010
CTH01020
CTH01030
CTH01040
CTH01050
CTH01060
CTH01070
CTH01080
CTH01090

CTH01110
CTH01160
CTH01190
CTH01200
CTH01210
CTH01220

R1706

PAGE 1

77/07/08. 10.52.40

FTR 4.6+428

73/74 OPT=1

SUBROUTINE COSIN

```
SUBROUTINE COSIN(X, SX, CX)
SX=SIN(X)
CX=COS(X)
RETURN
END
```

1

5

```

1      REAL FUNCTION J1(X)
2      T=D.
3      A=O.
4      T=D.
5      Z=X
6      X=ABS(X)
7      IF(X-LE-.3)GO TO 5
8      IF(X-GE.3)GO TO 10
9      GO TO 15
10     K=2
11     Y=X/3.
12     A=-.56249985*(Y**2)+.2193573*(Y**4)-.03954289*(Y**6)
13     A=(A+.00443319*(Y**8)-.00031761*(Y**10)+.0001109*(Y**12))*X
14     J1=A
15     GO TO 15
16     GO TO 15
17     V=3./X
18     F=.79788456+.0000156*Y+.01559667*(Y**2)+.00017105*(Y**3)
19     F=F-.00249511*(Y**4)+.00118553*(Y**5)-.00020033*(Y**6)
20     T=X-2.35619449+.12499612*(Y)+.03005650*(Y**2)-.00637879*(Y**3)
21     T=T+.0007434*(Y**4)+.00079276*(Y**5)-.00029166*(Y**6)
22     J1=F*COS(T)/X**5
23     IF(Z-LT-D.)J1=-J1
24     RETURN
25     END

```

```

CTH01570
J1 00030
J1 00040
J1 00050
J1 00060
J1 00070
J1 00080
J1 00090
J1 00100
J1 00110
J1 00120
J1 00130
J1 00140
J1 00150
J1 00160
J1 00170
J1 00180
J1 00190
J1 00200
J1 00210
J1 00220
J1 00230
J1 00240
J1 00250

```

```

1      FUNCTION FTC(X)
COMMON A1PA2,PK1(400),COSX(400),SINX(400),R,KD,IFSW,IITIME,OUTR(200),CTHO1240
*0),OUTI(2000),RO,A,K1,K2,FMAY,ALPHAD,P1,P2,BOVERA,SMRO,SIG,CC ,
1RFL,XYZ,D
5      DIMENSION DU*(1000)
REAL KD
REAL K1,K2
GO TO (10,20,30,40) IFS#
10     0-R % SIG=SIGMA(G)
IF(SINX(IITIME)-GE-.00001) GO TO 12
11     IF(R.NE.RO) GO TO 22
FTC=1.0/RO/(1.+(SIG/2.))**2)
RAD=KD*RO
GO TO 13
15     FTC=DUM(IITIME)=0.0
GO TO 15
12     RAD =SQRT((R
FTC=BK1(IITIME)*EXP(-ALPHAD*RAD)/RAD+SINX(IITIME)/(1.+(SIG/2.))**2)
RAD=KD*(RAD+R)
13     CALL COSIN(RAD,SX,CX)
DUM(IITIME)=FTC*SX
FTC=FTC*CX
GO TO 15
20     FTC=DUM(IITIME)
15     IITIME=IITIME+1
RETURN
30     FUNC=A1PA2**((SMRO*2.*SINX(X)
FTC=OUTR(IITIME)+FUNC*SMRO*2.*COSH(X)
GO TO 15
40     FUNC=A1PA2**((SMRO*2.*SINX(X)
FTC=OUTI(IITIME)+FUNC*SMRO*2.*COSH(X)
GO TO 15
END

```

```

CTHO1230
CTHO1240
CTHO1250
CTHO1270
CTHO1280
CTHO1290
CTHO1300
CTHO1310
CTHO1330
CTHO1340
CTHO1350
CTHO1360
CTHO1370
CTHO1380
CTHO1390
CTHO1400
CTHO1420
CTHO1430
CTHO1440
CTHO1450
CTHO1460
CTHO1470
CTHO1480
CTHO1490
CTHO1500
CTHO1510
CTHO1520
CTHO1530
CTHO1540
CTHO1550
CTHO1560

```

```

1 FUNCTION SPEED(S,T,P)
  C SOUND SPEED IN CM/SEC
  C S SALINITY IN PARTS PER THOUSAND
  C T TEMP. IN DEGREES C
  C P PRESSURE IN KG/CM**2 1 ATM FOR 6=980 CM/SEC**2
  VT=4.5721*T-4.4532E-2*T**2-2.6043E-4*T**3+7.9851E-6*T**4
  VP=1.60272E-1*P+1.0268E-5*P**2+3.5216E-9*P**3-3.3603E-12*P**4
  VS=1.39799*(S-35)+1.69202E-3*(S-35)**2
  VSTP=(S-35)*(-1.244E-2*T+7.7711E-7*T**2+7.7016E-5*P-1.2943E-7*P**2+ALS00010
12+3.158E-8*P**3)+P**2*(-2.5294E-7*T+1.8563E-9*T**2)-P**3+1.9646E-10*TALS00110
15283E-8*T**3)+P**2*(-2.5294E-7*T+1.8563E-9*T**2)-P**3+1.9646E-10*TALS00110
SPEED=1649.14+VT+VP+VS+VSTP
SPEED=SPEED*100.
RETURN
END
15

```

```
1 FUNCTION E1(X)  
A=X  
CALL EXPI(RES,A,AUX)  
C EXPI IS IN THE IBM SCIENTIFIC SUBROUTINE PACKAGE (SSPLIB/UN=RAYFTN)  
E1=RES  
5 RETURN  
END
```

```

1      FUNCTION ALF(S,T,F,P)
      C      SMALL SIGNAL ABSORPTION COEFFICIENT IN NEPERS/CM
      C      ONE NEPER IS 8.686 DB
      C S - SALINITY IN PARTS/THOUSAND
      C T - TEMP IN DEGREES C
      C F - FREQ IN KHZ
      C P - PRESSURE KG/CM**2 = 1 ATM IF 6=980 CM/SEC**2
      IF(S.GT.0.0) GO TO 1
      A = 6.0 - 1520.0/( T + 273.0 )
      FT=21.9*10.0**A
      ALF=((2.34E-6*S*FT**F)/(FT*FT**F) + 3.38E-6**F/FT)*
      1 (1.0-6.54E-4*P)
      ALF=ALF/100 $ RETURN
      1 A1=1.7760
      A2=32.768
      A3=6.54E-04
      A4=0.018587
      A5=0.026847
      E=2.7182818285
      CF=1.0936133E-05/(20.0*ALOG10(E))
      TEMP=T
      FT=21.9*10.0**((6.0*TEMP+118.0)/(TEMP+273.0))
      FKNZ=F
      FKNZ2=FKNZ*FKNZ
      FKNZ3=FKNZ*FKNZ2
      ALFADB=(A1*FKNZ**1.5/(A2+FKNZ3))+(1.0-A3*P)/(1.0*A2/FKNZ3)**((A4
      **S*FT*FKNZ2/(FKNZ2+FT**F))+A5*FKNZ2/FT)
      ALF=ALFADB*CF
      RETURN
      END
15
20
25
30

```

SUBROUTINE INEGR 73/74 OPT=1

```
1 SUBROUTINE INEGR(X,BOT, TOP,INT)
  XINT=INT
  H=(TOP-BOT)/XINT
  X=FTC(BOT)
  W=4.D
  5 9=BOT+H
  N=INT-1
  DO 1 K=1,N
  10 A=FTC(B)
  A=A*W
  X=X+A
  B=B+H
  W=6.-W
  15 X=X+FTC(TOP)
  X=X*H/3.
  RETURN
  END
```


APPENDIX B

In this appendix is supplied for reference a FORTRAN listing of the main program and required subprograms used to evaluate the Lockwood model. A description of the model may be found in Reference 5.

This program has also been implemented on a programmable calculator (Texas Instruments SR-52).

```

1 C PROGRAM HORN(TAPES,TAPES)
2 C THIS PROGRAM CALCULATES THE AXIAL SOURCE LEVEL OF A PARAMETRIC
3 C TRANSMITTING ARRAY BY APPLYING GEOMETRICAL CORRECTION FACTORS
4 C TO LEVELS BASED ON THE 1971 WELLEN-MOFFETT THEORY. A FACTOR
5 C IS APPLIED ONLY TO A PORTION OF THE INTERACTION RANGE AND IT IS
6 C NECESSARY THAT ATTENUATION IN THIS PORTION BE INSIGNIFICANT IF THE
7 C OBSERVATION POINT IS IN THE NEARFIELD.
8 C
9 C
10 C THE INPUTS ARE SO FORMATTED THAT THE SAME INPUT FILE MAY BE
11 C USED FOR BOTH WILLET AND HORN. THEREFORE, CERTAIN VARIABLES,
12 C SPECIFICALLY IJ, RHO, M, XNN, AND BOVERA, ARE DUMMYS. FOR
13 C GENERAL COMPATIBILITY, THE INPUT SHOULD BE PREPARED FOLLOWING THE
14 C INSTRUCTIONS FOR WILLET.
15 C
16 C FK1 AND FK2 ARE IN HZ, SL1 AND SL2 ARE FPS RE 1 MICKROPASCAL AT 1 M, A
17 C IS RADIUS IN METERS, TEMP IS IN DEGREES CELSIUS, AND DEPTH IS IN
18 C METERS.
19 C
20 C EXTERNAL FTC
21 C COMMON TUARD, DSR, CHI
22 C REAL LSD
23 C NAMELIST/INPUTS/FK1,FK2,SL1,SL2,A,RHO,TEMP,S
24 C ARSINH(X)=ALOG(X+(X*X+1)**.5)
25 C PI=3.14159265
26 C READ(5,2)FK1,FK2,SL1,SL2,A,RHO,TEMP,S
27 C IF(FK1.EQ.0.)GO TO 12
28 C READ(5,301)IJ,M,XNN,BOVERA,DEPTH
29 C PRESS=DEPTH*.097+1.
30 C WRITE(6,INPUTS)
31 C FORMAT(8E10.3)
32 C FOOVF=(FK1+FK2)/ABS(FK1-FK2)/2.
33 C FO=(FK1+FK2)/2./1000.
34 C ALPHA=ALF(S,TEMP,FO,PRESS)
35 C CO=SPEED(S,TEMP,PRESS)/100.
36 C RO=(FK1+FK2)*2.*PI/CO*(A/2.)*2
37 C RO=RO/.9144
38 C SPL=(SL1+SL2)/2.-96.2227
39 C FFORMAT(2I10,3F10.0)
40 C CO=CO*100.
41 C READ(5,102) R
42 C FFORMAT(F11.4)
43 C IF(R.EQ.0.)GO TO 999
44 C R=R/.9144
45 C DSR=1./FOOVF
46 C TUARD=2.*RO*91.44*ALPHA
47 C UMAX=ARSINH(R/RO)
48 C EPS=10.**((SPL/20.)/CO/CC
49 C AK=3.83*FO
50 C CHI=3.5*EPS*AK
51 C USMRD=ARSINH(FOOVF)
52 C CALL FACTOR(FAC,ICASE,R,RO,FOOVF)
53 C IF(ICASE.LE.2) GO TO 500
54 C CALL INTGR(FTC,ROINT,D.,UMAX,30)
55 C UTST=UMAX
56 C PE=FAC*ROINT*CHI/2.*DSR*DSR
57 C EXINT=D.
58 C GOTO 600
59 C CALL INTGR(FTC,ROINT,D.,US*RO,30)

```

NF100020
NF100030

NF100040
NF100050

NF100070

NF100090
NF100100
NF100110
NF100120
NF100140
NF100150
NF100160

NF100190

NF100210
NF100220
NF100230
NF100240

NF100250
NF100260
NF100270
NF100280

NF100290
NF100300
NF100310
NF100320
NF100330

NF100340
NF100350
NF100360
NF100370

```

60      UTST=USMRO
        CALL INTGR(FTC,EXINT,USMRO,UMAX,30)
        PE=(FAC*ROINT+EXINT)*CHI/2.*DSR*DSR
        CONTINUE
        SPLD=SPL-20.*ALOG10(R)+20.*ALOG10(PE)+97.
        CHI=1.E-4
        TUARO=1.E-4
65      CALL INTGR(FTC,ISTINT,J,UTST,30)
        IF(TSTINT/ROINT.GE..89.DC.FAC.LT.1.27) GO TO 103
        WRITE(6,110)
        FORMAT("WARNING: SIGNIFICANT ATTENUATION IN REGION TO WHICH FACTOR
110      115 APPLIED")
        R=R*.9144
        SPLD=SPLD+20.*ALOG10(R)
        PE=20.*ALOG10(PE)
70      WRITE(6,109) R,SPLD,PE
        FORMAT(" R=",F11.4,"SLD=",F11.4,"PARAMETRIC EFFICIENCY=",F11.4)
75      WRITE(6,112)P,ICASE,FAC
        FORMAT("R=",F11.4,"ICASE=",I1,"FAC=",F11.4)
        GO TO 100
12      CONTINUE
      END

```

NF100380
NF100390
NF100400
NF100410

NF100420
NF100430

NF100470
NF100480
NF100490
NF100500

73/74 OPT=1

FUNCTION FTC

```

FTC00010
FTC00020
FTC00030
FTC00040
FTC00050
FTC00060
FTC00070
FTC00080
FTC00090
FTC00100

```

```

FUNCTION FTC(U)
COMMON TUARO,DSR,CHI
A=SINH(U)
B=DSR*A
C=-TUARO*A
D=CHI*U/2.
FTC=EXP(C)/(1.+D**2)
FTC=FTC*SQRT((1.+A*A))/(1.+B*B)
RETURN
END

```

```

1
5
10

```

FUNCTION ALF

```

1  FUNCTION ALF(S,I,F,P)
    C SMALL SIGNAL ABSORPTION COEFFICIENT IN NEPCERS/CM
    C ONE NEPER IS 8.686 DB
    C S - SALINITY IN PARTS/THOUSAND
    C T - TEMP IN DEGREES C
    C F - FREQ IN KHZ
    C P - PRESSURE KG/CM**2 = 1 ATM IF 6=980 CM/SEC**2
    IF(S.GT.0.0) GO TO 1
    A = 4.0 - 1520.0/( T + 273.0 )
    FT=21.9*10.0**A
    ALF=((2.34E-6*S*FT*F*F)/(FT*FT*F*F) + 3.38E-6*F*F/FT)*
    1 (1.0-6.54E-4*P)
    ALF=ALF/100 $ RETURN
1  A1=1.7760
    A2=32.768
    A3=6.54E-04
    A4=0.018587
    A5=0.026847
    E=2.7182818285
    CF=1.0936133E-05/(20.0*ALOG10(E))
    TEMP=T
    FT=21.9*10.0**((6.0*TEMP+119.0)/(TEMP+273.0))
    FKHZ=F
    FKHZ2=FKHZ*FKHZ
    FKHZ3=FKHZ*FKHZ2
    ALFADB=(A1+FKHZ**1.5/(A2+FKHZ3))+(1.0-A3*P)/(1.0+A2/FKHZ3)**(A4
    **S*FT*FKHZ2/(FKHZ2+FT*FT))+A5*FKHZ2/FT)
    ALF=ALFADB*CF
    RETURN
    END
30

```

```

ALS00010
ALS00020
ALS00030
ALS00040
ALS00050
ALS00060
ALS00070
ALS00080
ALS00090
ALS00100
ALS00110
ALS00120
ALS00130
ALS00140
ALS00150
ALS00160
ALS00170
ALS00180
ALS00190
ALS00200
ALS00210
ALS00220
ALS00230
ALS00240
ALS00250
ALS00260
ALS00270
ALS00280
ALS00290
ALS00300

```

SUBROUTINE INTGRT 73/74 OPT=1

```

1      SUBROUTINE INTGRT(FTC,X,BOT,TOP,INT)
      C*****27 MARCH 1975*****
      EXTERNAL FTC
      XINT=INT
      N=(TOP-BOT)/XINT
      X=FTC(BOT)
      M=4.
      B=BOT+H
      N=INT-1
      DO 1 K=1,M
      A=FTC(B)
      A=A*N
      X=X+A
      B=B+H
      M=6.-M
      X=X+FTC(TOP)
      X=X+H/3.
      RETURN
      END
5
10
15      1

```

```

CIN0310
CIN0020
CIN0330
CIN0040
CIN0050
CIN0360
CIN0070
CIN0080
CIN0090
CIN0100
CIN0310
CIN00120
CIN00130
CIN03140
CIN03150
CIN03160
CIN03170
CIN00180
CIN03190

```

```

1  SUBROUTINE FACTOR(FAC, ICASE, R, RO, FOOVF)
   ROMIN=RO/FOOVF
   SMRO=RO*FOOVF
   RC=(SMRO/2.)*(-1.+SQRT(1.+4.*R/SMRO))
   IF(R-6E-2.*SMRO) ICASE=1
   IF(R-LT-2.*SMRO) ICASE=2
   IF(R-LT-SMRO) ICASE=3
   IF(R-LT-RO+ROMIN) ICASE=4
   IF(R-LT-RO) ICASE=5
   IF(R-LT-ROMIN) ICASE=6
   GO TO (10,20,30,40,50,60), ICASE
   FAC=R/SMRO*ALOG(R/(R-SMRO))
   RETURN
10  FAC=R/SMRO*(ALOG(R/(R-RC)))+(SMRO-RC)/RC
   RETURN
15  FAC=ALOG(R/(R-RC))+SMRO/R*(R-RC)/RC
   RETURN
20  FAC=ALOG(R/ROMIN)-(R-RO)**2/R/ROMIN+1.
   RETURN
25  FAC=ALOG(R/ROMIN)+1.
   RETURN
30  FAC=R/ROMIN
   RETURN
   END

```

```

1  FUNCTION SPEED(S,T,P)
   C SOUND SPEED IN CM/SEC
   C S SALINITY IN PARTS PER THOUSAND
   C T TEMP. IN DEGREES C
   C P PRESSURE IN KG/CM**2 1 ATM FOR G=980 CM/SEC**2
   VT=4.5721*T-4.4532E-2*T**2-2.6045E-4*T**3+7.9851E-6*T**4
   VP=1.60272E-1*P+1.0268E-5*P**2+3.5216E-9*P**3-3.3603E-12*P**4
   VS=1.39799*(S-35)+1.69202E-3*(S-35)**2
   VSTP=(S-35)*( -1.244E-2*T+7.7711E-7*T**2+7.7016E-5*P-1.2943E-7*P**AL500090
12+3.158E-8*P*T+1.579E-9*P*T**2)+ P*(-1.5407E-4*T+7.4812E-6*T**2+6.AL500100
15283E-8*T**3)+P**2*(-2.5294E-7*T+1.8563E-9*T**2)-P**3+1.9646E-10*TAL500110
   SPEED=1449.14+VT*VP+VS+VSTP
   SPEED=SPEED*100.
   RETURN
   END
15

```